Morphology and ultrastructure of the midgut gland ("hepatopancreas") during ontogeny in the common spider crab *Maja brachydactyla* Balss, 1922 (Brachyura, Majidae).

Diego Castejón[1*], Guiomar Rotllant[1], Javier Alba-Tercedor[2], Maria Font-i-Furnols[3], Enric Ribes[4], Mercè Durfort[4], and Guillermo Guerao[5]

[1]CSIC, Institut de Ciències del Mar, Passeig Marítim de la Barceloneta 37-49. 08003 Barcelona (Spain).

[2]Departamento de Zoología, Facultad de Ciencias, Universidad de Granada, Campus de Fuentenueva, Av. de Fuente Nueva s/n. 18071 Granada (Spain).

[3]IRTA, Qualitat del Producte, Finca Camps i Armet. 17121 Monells, Girona (Spain).

[4]Unitat de Biologia Cel·lular, Departament de Biologia Cel·lular, Fisiologia i Immunologia, Facultat de Biologia, Universitat de Barcelona, Diagonal 645. 08028 Barcelona (Spain).

[5]Independent Researcher. Barcelona (Spain).

Short title: *Maja brachydactyla* midgut gland morphology

***Corresponding author:** Diego Castejón. E-mail: diego.castejon.dcb@gmail.com; phone: +34 681 154 398; postal address: CSIC, Institut de Ciències del Mar, Passeig Marítim de la Barceloneta 37-49. 08003 Barcelona (Spain).

Abstract.

We studied the anatomy and cytology of the midgut gland (MGl) of the common spider crab *Maja brachydactyla* Balss 1922 at several life stages (zoea, megalopa, first juvenile, and adult) using dissection, histology, electron microscopy, computed tomography, and micro-computed tomography (micro-CT). In newly hatched larvae, 14 blind-end tubules formed the MGl. The length of the tubules increases during the larval development. In the late megalopa, the number of tubules also increases. In adults, 35,000 to 60,000 blind-end tubules comprise the MGl. In all life stages, a square-net network of muscle fibers surround the tubules. We describe five cell types in the MGl in all larval stages, which have a similar location, histology, and ultrastructure in larvae and adults: embryonary (E-) cells, resorptive (R-) cells, fibrillar (F-) cells, blister-like (B-) cells, and midget (M-) cells. Major difference between larval and adult cells is the larger size of the adult cells. Microapocrine secretion occurs from the microvilli of the B-cells. No ultrastructural changes were observed, which suggests that the function of each cell type might be similar in all life stages. The role of each epithelial cell type in larvae and adults is discussed.

Keywords: Crustacea; larval development; digestive system; micro-CT; microapocrine secretion

1. Introduction

The midgut gland (MGl), which is formed by several blind-end tubules, is the largest digestive organ in Decapoda (Gibson and Barker, 1979; Felgenhauer, 1992; Icely and Nott, 1992). The MGl traditionally has been known as “hepatopancreas” (Milne-Edwards, 1834a, b; Schlegel, 1911; Van Weel, 1974; Gibson and Barker, 1979; Davie et al., 2015). Recently, Cervellione et al. (2017b) concluded that the term “hepatopancreas” is inappropriate because the MGl inherently differs from the liver and pancreas of vertebrates, and proposed the term “perigrastric organ”. In this study, however, we used the term “midgut gland” because it has been used extensively in other studies, and the use of “perigrastric organ” remains under discussion.

The epithelium of the tubules that form the MGl comprises several cell types: E-cells (embryonic), which are involved in cell division and differentiation, F-cells (fibrillar), which have “striated” cytoplasm, R-cells (resorptive), which are rich in lipid vacuoles and glycogen, B-cells (blister-like), which are characterized by a very large supranuclear vacuole (Loizzi, 1971; Al-Mohanna and Nott, 1989; Felgenhauer, 1992; Icely and Nott, 1992), and M-cells (midget), which are short cells that do not reach the organ lumen (Al-Mohanna et al., 1985a). The morphology, ultrastructure, and role of those cells in adult decapods have been well studied (Van Weel, 1974; Gibson and Barker, 1979; Vogt, 1996; Hu and Leung, 2007); however, the larval stages have received significantly less attention. Furthermore, few studies have investigated the ontogeny of the midgut gland in brachyuran crabs (Li and Li, 1998).

The general morphology of the MGl in adults and the first zoeal stage of spider crabs of the genus *Maja*, has been described by (Milne-Edwards, 1834b) and (Schlegel, 1911), respectively. In those studies, a detailed cellular description of the MGl and the

functions of the cell types were not provided. In this study, we described the MGl of the common spider crab *Maja brachydactyla* Balss 1922 at several life stages (zoea, megalopa, first juvenile, and adult) using dissection, histology, transmission electron microscopy, scanning electron microscopy, computed tomography, and micro-computed tomography (micro-CT). The role of each epithelial cell type during the development is discussed.

2. Material and methods

2.1 Broodstock and larval culture systems

The adults were caught in the Atlantic Ocean by order to fishery companies (LONXANET, CADEMAR), transported to the Institut de Recerca i Tecnologia Agroalimentàries facilities (IRTA, Sant Carles de la Ràpita, Tarragona, Spain), and dissected upon arrival or kept as broodstock. The broodstock was kept in 2,000-L cylindrical tanks that were connected to a recirculation unit (renewal rate = 3.5 m^3 h^{-1}) and maintained at constant environmental conditions: 18 ± 1 °C, salinity of 35 ± 1, photoperiod = 12 h light photoperiod, and fed frozen mussels (*Mytilus* sp.). The larvae were recovered 12 h after hatching and maintained in 600-mL glass beakers that were placed inside 360-L tanks (96 x 96 x 40 cm), which were used as incubation chambers that were maintained at the following conditions: 21 ± 1 °C, salinity = 35 ± 1, 12 h light photoperiod, and fed *Artemia* sp. nauplii (INVE Aquaculture Nutrition, Salt Lake UT, USA). The larvae and first juvenile were sampled at the start of each stage: zoea I as newly hatched larvae (0 days - d), zoea II in 3 d, megalopa in 6 d, and first juvenile stage in 11-12 d.

2.2 Gross morphology

Six adults were sedated before dissection by placing them for 30-60 min in a bucket filled with crunched ice. To expose the midgut gland (MGl), a pair of small pliers were used to remove the carapace of the adults. The entire fresh MGl of each specimen was weighed. Samples of each MGl were taken, weighed, and fixed in 4% formaldehyde. To calculate the relative weight change caused by the fixing process, the fixed samples were weighed again. Subsamples of known weight (15-60 mg) were taken to count the number of tips of the blind-end tubules, which was used to calculate the density of tubules (tubules per unit mass). The density was used to extrapolate the number of tubules per MGl. Samples were weighed on a Mettler Toledo AE200 balance (range = 0 - 205 g, precision = 0.1 mg). Observations were made using a Nikon SMZ800 stereomicroscope.

The larvae and first juvenile were sampled at the start of each stage, within approx. 15 h after the molt, and immediately fixed in 4% formaldehyde. Larvae were dissected using teasing needles. In each stage, 4-6 MGls were extracted, photographed, and measured using AnalySIS® software tools (Soft Imaging System, Münster, Germany). Measurements were performed as described, below (see Suppl. Fig. 1):

2.2.1. Ventral sub-lobule (VSL): total length (TL) and maximum width (MW).

2.2.2. Lateral tubules were defined as either external (ET) or internal (IT) based on their position toward the MGl center. For the ET, the following measurements were taken: total length (ETl) and total width (ETw); for the IT, the measurements were total length (ITl) and total width (ITw). The lateral tubules project at diverse angles; therefore, total width was measured as the basal line that separates the lateral tubule from the central tubule, and total length was measured as the maximum perpendicular distance from the basal line to the tip of the lateral tubule (Suppl. Fig. 1 for details).

2.2.3. Dorsal sub-lobule (DSL): total length (DSl), width (DSw), and height (DSh).

The data were analyzed using R version 3.2.0 (R Development Core Team, 2015). A One-way ANOVA was performed for each of the measurements (TL, MW, DSl, DSw, DSh, ETl, ETw, ITl, or ITw). Statistical comparisons among life stages (zoea I, zoea II, megalopa, first juvenile) after the detection of significant differences were performed using a Tukey HSD test. Normality and homogeneity were tested by Shapiro-Wilk and Levene Tests. The critical level (α) for the rejection of the null hypothesis was 0.05.

2.3 Histology

In larvae and first juvenile, the specimens were fixed as a whole. In adults, the material fixed were small pieces of the MGl. Davidson's fixative (ethanol absolute: seawater: 37% formaldehyde: glycine: glacial acetic acid in proportion 3: 3: 2: 1: 1) was used for all samples. The fixation process lasted 24 h, after which, the fixed tissues were preserved in 70% ethanol. Dehydration and paraffin infiltration were performed using an automatic tissue processor (Myr, Spain). The blocks were formed in a paraffin processor (Myr, Spain) and a microtome (Leica RM2155) was used to obtain 2-µm sections. The staining procedures were as follows: 1. Hematoxylin-Eosin (HE) to reveal the general morphology of the tissue. 2. Periodic Acid–Schiff (PAS) contrasted with Methylene Blue to reveal the presence of polysaccharides, neutral mucopolysaccharides, and the structure of the cuticle line. 3. Mallory's trichrome stain (Acid Fuchsine, Orange G and Aniline Blue stains) to reveal the structure of the muscular and connective tissues. The stained sections were observed under an optical microscope (Leica LB30T 111/97), photographs were taken with a camera (Olympus

DP70), and the image analyzing system software was DP Controller 2.1.1.83 with DP Manager 2.1.1.163 (Olympus Corporation, Germany).

2.4 Electron microscopy (TEM and SEM)

For larval and first juvenile stages, the material fixed were entire specimens of each stage for transmission electron microscopy (TEM), and dissected MGl of the first zoeal stage for scanning electron microscopy (SEM). For adult specimens, the material fixed were small pieces of the MGl for TEM and SEM. Fixative solution was 2% paraformaldehyde and 2.5% glutaraldehyde in a cacodylate buffer (0.1 mol L^{-1} pH 7.4). The fixation process required approx. 12 h at 4 °C and constant darkness. Fixed samples were rinsed twice with cacodylate buffer (0.1 mol L^{-1}, pH 7.4), post-fixed in 1% osmium tetroxide, and dehydrated by increasing series of acetone solutions. For TEM, the samples were embedded in Spurr's resin, semi-thin sections were obtained using a Leica UCT ultra-microtome and were stained by Bromophenol Blue. Ultra-thin sections (60-nm) were performed using the ultra-microtome and counterstained with uranyl acetate and lead citrate. Observations were made using a JEOL EM-1010 transmission electron microscope (tungsten filament, 80 kV). For SEM, after critical-point drying, the post-fixed samples were mounted on SEM stubs using self-adhesive carbon stickers and covered with a carbon coating. Observations were made using a JEOL JSM-7001F scanning electron microscope (15 kV). The post-fixative treatment and TEM and SEM observations were performed at CCiTUB (Hospital Clinic, University of Barcelona, Barcelona).

2.5 Computed tomography and micro-computed tomography (micro-CT)

For the computed tomography, two protocols were used. For adults, one male and one female were scanned using a General Electric HiSpeedZx/I (GE Healthcare,

Boston, Massachusetts, USA). The scanning parameters were as follows: helical acquisition, pitch 1, 140 kV, 150 mA, displayed field of view 250 mm, 3 mm thickness, and reconstruction algorithm STD+. Image analysis was performed using Centricity Radiology RA600 v.7 software (GE Medical Systems Information Technologies, Inc., Milwaukee, WI, USA). The tomography of the adult specimens was performed at the Institut de Recerca i Tecnologia Agroalimentàries (IRTA) facilities of Monells (Girona, Spain). For the larvae, zoeae were fixed in 2% paraformaldehyde and 2.5% glutaraldehyde in a cacodylate buffer (0.1 mol L^{-1}, pH 7.4), and megalopae were fixed in 70% ethanol. The fixed larvae were preserved in 100% isopropanol. Thereafter, the specimens were placed in a solution of 1% iodine in absolute ethanol for 72 h, submerged in hexamethyldisilazane for 4 h, and air-dried overnight. To kept the specimens in the sample holder, several methods have been described (Alba-Tercedor and Sáinz-Cantero, 2012; Alba-Tercedor, 2014). For the zoea larvae, the most effective method was to use cyanoacrylate to glue the animal to the tip of a nylon filament line (200-µm diam.). Megalopa were mounted inside a hollowed piece of BASOTECT® (melamine resin foam, created by the Chemical Company BASF). To prevent the forced refrigerated air from moving the samples during the scan process, each sample was enclosed within a plastic straw. The Basotect material has a very low density, is very transparent to X-Rays and, therefore, can be eliminated easily during the segmentation procedure (Alba-Tercedor and Alba-Alejandre, 2017). Scans were performed using a SkyScan 1172 high resolution microtomographer (Bruker microCT - formerly, Skyscan -, Kontich, Belgium), a Hamamatsu 80/250 source, and a VDS 1.3Mp camera. For the zoea, the scanning parameters were as follows: isotropic voxel size of 1.48 µm per pixel, 49 kV, 78 µA, 0.3° rotation step, and 180º rotation scan. For the megalopa, the scanning parameters were as follows: isotropic voxel size of 1.47 µm per pixel, 54 kV,

85 μA, 0.5° rotation step, and 180º rotation scan. For primary reconstructions and the "cleaning" process for obtaining the datasets of cross-sectional images ('slices'), we used the latest versions of Bruker microCT, formerly Skyscan (www.skyscan.be), software (NRecon, DataViewer, CTAnalyser). Volume measurements were obtained using Skyscan software CTVox. For a more detailed description of the procedures, see (Alba-Tercedor, 2014), which were performed at the Department of Zoology, University of Granada, Spain.

3. Results

General morphology. The midgut gland (MGl) of *M. brachydactyla* larvae is located in the middle of the cephalothorax, and partially covers the pyloric stomach (Fig. 1; Suppl. Fig. 2A-B, D-E). The gross morphology is similar throughout larval development (Figs. 1; 2B-C; 3; Suppl. Fig. 2). The MGl presents two asymmetrical lobules (right and left), each of which is subdivided into a dorsal and a ventral sub-lobule (Figs. 1; 2B-C; Suppl. Fig. 1). The dorsal sub-lobule is flattened laterally and composed of a single anterior tubule and a pair of posterior tubules. The ventral sub-lobule has a "trident-like" shape consisting of a single posterior tubule and three anterior tubules: external, central, and internal (Fig. 2B-C; Suppl. Fig. 2). The pyloric stomach lies above the internal tubules (Fig. 1; Suppl. Figs. 2C, F; 3C-D). The MGl of the newly hatched larvae has fourteen tubules. New tubules start to develop as small buds in the late megalopa (around the ninth or tenth day of development at 21°C). The growth of MGl is allometric: the tubules elongate significantly throughout larval development, but width increased marginally (Table 1, Fig. 3). Thus, the ratio between length and width increases significantly from two in the newly hatched larvae to four in the newly molted juvenile (right lobule: $F_{3,16}$= 12.46 $p < 0.001$; left lobule: $F_{3,16}$ = 24.43 $p < 0.001$).

206 The MGl of adult *M. brachydactyla* occupies the whole cephalothoracic cavity
207 (Fig. 2A; Suppl. Fig. 3A-B) and is divided into two main lobes: right and left. Each lobe
208 extends within the cephalothoracic cavity into three projections: anterior, lateral, and
209 posterior (Fig. 2A). On average, the MGl of the adults is composed of 46,000 blind-end
210 tubules (range = 35,000 - 60,000) among specimens that have a mean carapace length =
211 135 ± 8 mm at a density of 2.3 ± 0.8 tubules per mg of fresh MGl. The tubules are
212 branched in a coral-like pattern (Fig. 2D; Suppl. Fig. 6). In adults, thin muscle fibers
213 surround the tubules. The orientation of the muscle fibers is either circular or
214 longitudinal (Fig. 2E). The intimate relationship between the epithelial cells and muscle
215 fibers implies that the epithelium forms basal folds that fit with the fibers (Figs. 2E; 4F).
216 The circular muscle fibers form parallel rings that are separated by intervals of 47.58 ±
217 8.33 µm along the tubule length, and the longitudinal muscle fibers are parallel to the
218 longitudinal axis at intervals of 9 ± 2 µm. The longitudinal and circular muscle fibers
219 are connected and form a rectangular network (Fig. 2E). In the larvae, the morphology
220 is similar, although the muscle fibers are thinner than in the adults (Suppl. Fig. 4).

221 *Morphology and ultrastructure.* The morphology of the epithelial cells is similar
222 in the larvae and first juveniles. Therefore, here, these stages are described together as
223 "immature stages". The MGl of *M. brachydactyla* is lined by a simple columnar
224 epithelium with microvilli. In the immature stages, the height of the epithelial cells of a
225 single tubule ranges from 13 to 37 µm, which gives the lumen an irregular shape (Fig.
226 4D). In adults, cell height varies from 25 to 100 µm and the lumen is "X-shaped" (Fig.
227 4C). Five cell types have been identified in immature and adult stages (Figs. 4-5): *E-*
228 *cells* (embryonic), *R-cells* (resorptive), *F-cells* (fibrillar), *B-cells* (blister-like), and *M-*
229 *cells* (midget). The distribution of those cell types is similar in immature and adult
230 stages (Fig. 4A-B): 1) the distal tip is the "E-cell region" because the region is

populated by E-cells (Fig. 4E); 2) the “transitional region” comprises few F-cells and numerous R-cells, which have a cytoplasm that is poorly vacuolated; and 3) the proximal region is the “mature region”, where R-cells rich in lipid vacuoles and fully developed B-cells predominate. M-cells occur in the “transitional” and “mature regions” (Fig. 4A, F). The five cell types are described in detail, below.

E-cells. E-cells are hard to find; therefore, our observations were restricted to those made using histology. The E-cells of the immature and adult stages are similar and occur at the distal tip of the tubules. The E-cell cytoplasm is homogeneously stained and does not exhibit PAS-positive inclusions. The nucleus is large relative to the cell width (Figs. 4A-B; 5E). Several E-cells are reported in mitosis (Fig. 4E).

R-cells. The R-cell of the immature and adult specimens is columnar (Fig. 5) and is the main cell type of the MGl epithelium (85 ± 7% and 76 ± 6% of the cell population in immature and adult stages, respectively). The cytoplasm of the R-cells differs depending on the position of the R-cell along the tubule length: in the “transitional region”, it is homogeneously stained and contains few lipid vacuoles; however, in the “mature region”, the cytoplasm is rich in lipid vacuoles and PAS-positive inclusions (Fig. 4A-B). In adults, many R-cells resemble a “tower of lipid vacuoles” (Figs. 4C, F; 5G-H); however, in the immature stages, typically, the R-cells contain a single lipid vacuole that is located below the nucleus (Figs. 4D; 5C). The ultrastructural study shows a cell membrane that has a polarized organization (Fig. 6): 1) the apical membrane forms numerous undulated and slender microvilli (Fig. 6B-D), 2) the lateral membranes are more undulated and have larger apical cell-to-cell junctions in the adults than in the immature stages (Fig. 6B, D), and 3) the basal membrane is straight in the immature stages but, in adults, it occasionally forms folds (Fig.6E-F). In the immature stages, the cell apex is rich in mitochondria and rough

endoplasmic reticulum (RER) (Fig. 6B-C); however, in adults, the cell apex contains few organelles and vertical filaments associated with RER-like cisternae (Fig. 6D). The cell base contains abundant mitochondria and smooth endoplasmic reticulum (SER), which forms a branched, tubular net. The electron-density of the SER is higher in adults than it is in the immature stages (Fig. 6E-F). The SER tubes fuse with the basal membrane (Fig. 6H-I). In all life stages, Golgi bodies comprise flattened cisternae (Fig. 6G). Other structures observed in the R-cells of adults are multivesicular bodies, multilamellar bodies, and several kinds of vesicles that have single or double membranes and content that ranges from lucent to electron-dense. The R-cells of the adults also contain multivesicular and multilamellar bodies.

F-cells. In the immature and adult stages, the F-cells are similar and are distinguished by three features: 1) pyramidal shape, 2) highly stained cytoplasm that has fibrillar-like marks, and 3) the largest nucleus among the types of epithelial cells (Fig. 5B-C, G-H). F-cells are 7 ± 3% and 10 ± 2% of the cell populations in immature stages and adults, respectively. PAS positive inclusions are rare. The organization of the cell membrane is polarized: 1) the apical membrane forms numerous undulated and slender microvilli (Fig. 7B), 2) in adults, the lateral membranes are more undulated and form larger cell-to-cell junctions than are those in the immature stages, and 3) the basal membrane is generally straight (Fig. 7D). The cytoplasm is similar in all the life stages. The cytoplasm contains an extraordinary abundance of RER, mitochondria, and Golgi bodies. A large amount of RER cisternae occupy the cell from the base to the apex and exhibit three main types of organization: 1) random-like distribution (Fig. 7C), 2) parallel chains (Figs. 7B), and 3) concentric layers (Fig. 7D). Generally, the mitochondria are small (Fig. 7B-D), and the Golgi bodies have a distinctive morphology in this cell type because the cisternae are highly expanded and globular (Fig. 7B-C). In

281 immature stages and adults, the cell base contains a thin band comprising a tubular SEM
282 and mitochondria (Fig. 7D).

283 **B-cells**. B-cells have a similar morphology and ultrastructure in all the life
284 stages. B-cells are 8 ± 5% and 12 ± 5% of the cell populations in the immature stages
285 and adults, respectively. In the immature stages, the B-cells are taller than the adjacent
286 epithelial cells (Figs. 4B; 5D); however, in adults, the B-cells are shorter than the
287 adjacent epithelial cells (Figs. 4A; 5G-H). The key characteristic of the B-cells is the
288 very large central vacuole that occupies most of the cell volume. Generally, the vacuole
289 is rounded, single (not multiple, as in R-cells), and always has a supranuclear location
290 (never infranuclear, as occurs with some vacuoles in R-cells) (Figs. 4A-C; 5D, G-H).
291 The content of the vacuole is heterogeneous and stained as the lumen of the MGl (Figs.
292 4B; 5D). The ultrastructure of the B-cells is similar in the immature stages and adults.
293 The cell membrane is polarized: 1) the apical membrane forms short, undulated
294 microvilli (Fig. 8B, D), and 2) the lateral membranes are smooth, form apical cell-to-
295 cell junctions, and converge to form a cone/dome-shaped cell base (Fig. 8B-C). The
296 cytoplasm of the cell apex is electron-dense and filled with numerous lucent vesicles. It
297 is unclear whether those vesicles originate from the disintegration of the central vacuole
298 or, in contrast, merge into the central vacuole: many vesicles are fused with the apical
299 border of the central vacuole, and the diameter of the vesicles decreases toward the cell
300 apex (Fig. 8B). The cell base contains electron-dense cytoplasm that has numerous
301 cisternae of RER, few mitochondria, and some Golgi bodies, which are formed by
302 flattened cisternae (Fig. 8C, E). The contents of the central vacuole are similar in
303 immature stages and adults. These contents are highly heterogeneous and exhibits
304 lucent areas, electron-dense agglomerations, and lamellate formations (Fig. 8F). We
305 observed “micro-apocrine secretion” in the B-cells of adults: small lucent vesicles are

306 formed in the microvilli tip and are released into the lumen (MVs, Fig. 8A; numbers,
307 Fig. 8D).

308 **M-cells.** M-cells are the smallest cell type of the epithelium: 11.53 ± 1.50 µm in
309 width and 7.14 ± 0.48 µm in height. Therefore, they never reach the lumen of the MGl.
310 M-cells are more easily identified in adults (Fig. 4A, F) than they are in the immature
311 stages because of the shorter height of the epithelium in immature stages (Fig. 5B). M-
312 cells have been identified in the larval stages; e.g., zoea (Fig. 5B) and megalopa (Fig.
313 9C). They are rounded cells that have a central nucleus (Figs. 4F; 5B; 9C) and, at the
314 ultrastructural level, are similar in immature stages and adults (Fig. 9B-C). M-cells do
315 not exhibit polarity in cell membrane organization or organelle distribution. The cell
316 membrane is generally smooth, the cytoplasm lucent, and the density of organelles is
317 low (Fig. 9B-C). The mitochondria are small and dispersed around the nucleus (Fig. 9E-
318 F). The presence of endoplasmic reticulum is uncertain, although several lucent vesicles
319 that have different morphologies have been observed. The M-cells contain smooth and
320 rounded “electron-dense vesicles”, which have a diameter between 0.5 and 1.0 µm. The
321 content of the “electron-dense vesicles” varies from homogeneous to highly
322 heterogeneous and granular (Fig. 9B-C, F). Golgi bodies are few and small (Fig. 9D).
323 Few annulated lamellae have been observed in the cytoplasm, but physically separated
324 from the nucleus (Fig. 9E).

325 **Discussion**

326 This study investigated the gross morphology and ultrastructure of the midgut
327 gland of a brachyuran species at various stages of development. Micro-CT is a reliable
328 technique for studying the anatomy of crustacean larvae because it reveals the three-
329 dimensional morphology of the internal anatomy, including the MGl and other organs
330 (Castejón et al., 2018; Spitzner et al., 2018). In the larval stages, the gross morphology

of the MGl of *M. brachydactyla* comprises14 blind-end tubules. Previous studies based on histological observations reported that the MGl of several brachyuran species has a tubular organization in the larval stages, although the number of tubules was not reported (Schlegel, 1911; Trask, 1974; Nakamura, 1990; Jantrarotai and Sawanyatiputi, 2005). The MGl of larval *M. brachydactyla* is organized into dorsal and ventral sub-lobules, each of which comprises several tubules. The MGl of the larvae of the anomuran *Paralithodes camtschaticus* shows a similar organization (Abrunhosa and Kittaka, 1997). Brachyurans and anomurans are phylogenetically close (Scholtz and Richter, 1995); therefore, the gross morphology of the MGl in early development might be conserved in these two taxa. The development of the MGl in *M. brachydactyla* might be longer than it is in other brachyuran species because the new tubules start to develop in the late megalopa; in other species, however, the new tubules are apparent in the late zoeae (Nakamura, 1990; Jantrarotai and Sawanyatiputi, 2005). The MGl in adult *M. brachydactyla* is a large, orange-brown organ that is subdivided into three main lobules (anterior, posterior, and dorsal), which comprise thousands of tubules. The computed tomography confirmed the overall disposition of the MGl in the cephalothorax. A similar morphology has been reported in other brachyuran species; e.g., the eriphiid *Menippe rumphii* (Erri Babu et al., 1982), the gecarcinucid *Spiralothelphusa hydrodroma* (as *Parathelphusa hydrodromus*) (Reddy, 1937), the portunid *Scylla serrata* (Barker and Gibson, 1978), the ocypodids *Ocypode platytarsis* (Ramadevi et al., 1990) and *Uca uruguayensis* (Cuartas and Petriella, 2002), and the varunids *Neohelice granulata* and *Cyrtograpsus angulatus* (Cuartas and Petriella, 2002).

In *M. brachydactyla*, the organization of the tubules is similar in larval, juvenile, and adult stages. The main difference is the larger size of the epithelial cells in adults. The MGl has five types of epithelial cells: embryonary (E-) cells, resorptive (R-) cells,

356 fibrillar (F-) cells, blister-like (B-) cells, and midget (M-) cells, which occur in several
357 decapods including other brachyuran species (Gibson and Barker, 1979; Felgenhauer,
358 1992; Icely and Nott, 1992; Davie et al., 2015). In our study, the five cell types were
359 present in the larval stages of *M. brachydactyla*. Previous studies reported four or less
360 cell types in larval stages (Table 2). The epithelial cell types present in the MGl of *M.*
361 *brachydactyla* are heterogeneously distributed in different regions along the
362 longitudinal axis of the tubule. The distribution of cell types is similar in all life stages,
363 and is similar to the distribution observed in other decapods (Pillai, 1960; Loizzi, 1971;
364 Gibson and Barker, 1979; Hopkin and Nott, 1979; Al-Mohanna and Nott, 1989; Icely
365 and Nott, 1992). A degenerative "proximal zone" was described in *Orconectes virilis*,
366 *Procambarus clarkii*, and *Penaeus semisulcatus* (Loizzi, 1971; Al-Mohanna and Nott,
367 1989; Icely and Nott, 1992); however, this zone was not found in *M. brachydactyla* and
368 neither in the other crab species studied *Carcinus maenas* (Hopkin and Nott, 1980).
369 In *M. brachydactyla*, the epithelial cells of immature stages and adults have
370 similar ultrastructural features, which suggests that the function of each cell type is
371 similar in all life stages, and that the MGl of *M. brachydactyla* is ready for enzyme
372 production and food digestion at hatching. Newly hatched larvae of *M. brachydactyla*
373 are obligate feeders (Rotllant et al., 2010; Guerao et al., 2012) and can synthesize
374 several kinds of digestive enzymes which diversity increase during the ontogeny
375 (Rotllant et al., 2008; Andrés et al., 2010). Furthermore, we observed that the MGl of
376 the newly hatched larvae is rich in lipid vacuoles (Fig. 4D). The density of lipid
377 vacuoles in the MGl of decapods decreases strongly at starvation (Storch and Anger,
378 1983; Anger et al., 1985; Sánchez-Paz et al., 2007; Guerao et al., 2012; Cervellione et
379 al., 2017a); therefore, lipid storage might act as an energy reserve until the animal
380 catches its first prey.

In all life stages, the E-cells of *M. brachydactyla* are limited to the distal tip of the tubules and were observed in mitosis. E-cells differentiate into other cell types in the MGl (Gibson and Barker, 1979; Felgenhauer, 1992; Icely and Nott, 1992; Paquet et al., 1993; Li and Li, 1998). The ultrastructure of the epithelial cells of the MGl of *M. brachydactyla* (R-cells, F-cells, B-cells and M-cells) is similar in all the life stages and resembles to the reported in other decapod species; therefore, the functions of the epithelial cells of the MGl in *M. brachydactyla* might be similar to those suggested for other decapods viz., R-cells as absorptive, storage, and osmoregulatory cells, and F-cells are involved in the production of enzymes (Bunt, 1968; Loizzi, 1971; Gibson and Barker, 1979; Al-Mohanna et al., 1985a; Al-Mohanna and Nott, 1986, 1987, 1989; Felgenhauer, 1992; Paquet et al., 1993; Vogt, 1994; Li and Li, 1998).

The role of B-cells is unclear. Some authors have suggested that that B-cells are the last stage in the development of F-cells (Stanier et al., 1968; Al-Mohanna et al., 1985b; Al-Mohanna and Nott, 1986; Icely and Nott, 1992; Hu and Leung, 2007), which is consistent with our results. We observed epithelial cells that had features characteristic of both F- and B-cells. Specifically, the cytoplasm is rich in RER cisternae as in F-cells (Suppl. Fig. 5A-B) and contains a large supranuclear vacuole that has heterogeneous content as in B-cells (Suppl. Fig. 5A, C). Other studies have reported the existence of cells that have features of both F- and B-cell types (Stanier et al., 1968; Loizzi, 1971). The F-cells might represent a high investment of energy and resources. They are cells heavily rich in organelles and approx.10% of the cell population. Some of the investment might be recovered if the cytoplasmic content of the F-cells is recycled at the end of their functional life. If that is true, the B-cell vacuole might contain digested organelles from the previous F-cell stage. Since the vacuole of B-cells is released into the MGl lumen (Travis, 1955; Pillai, 1960; Barker and Gibson, 1977;

406 Franceschini-Vicentini et al., 2009), the vacuole release might permit the recycling of
407 the material from the previous F-cells stage. Supporting this hypothesis, we observed
408 several partially digested mitochondria in the vacuole of the cell that had features of
409 both F- and B-cells (Suppl. Fig. 5A, C). In addition, B-cells produced small vesicles
410 from the microvilli tip. That kind of secretion has been widely reported to occur in the
411 midgut tract of insects, which has been referred to as "microapocrine mechanism" or
412 "microapocrine route" (Ferreira et al., 1990; Cristofoletti et al., 2001; Silva et al., 2013;
413 Monteiro et al., 2014), but was not known to occur in the digestive system of decapods.
414 Sonakowska et al. (2015) mentioned "microapocrine" secretion in the midgut tract of
415 the caridean *Neocaridina heteropoda*; however, according to the published photographs,
416 the authors observed undulated microvilli, rather than secretory activity. In insects, that
417 type of secretion is associated with the release of digestive enzymes (Bolognesi et al.,
418 2001; Cristofoletti et al., 2001; Silva et al., 2013).

419 The role of M-cells is still unclear, although several hypotheses has been
420 proposed: 1) storage of proteins or enzymes (Al-Mohanna et al., 1985a; Nunes et al.,
421 2014), 2) endocrine cells because they are located near blood sinuses (Vogt, 1994), 3)
422 "blood cells" involved in the synthesis of hemocyanin or that have a phagocytic role
423 (Paquet et al., 1993), and 4) "basal cells" (Reddy, 1938) or "replacement cells" (Pillai,
424 1960) involved in mitosis and differentiation into other cell types. In our opinion, the
425 hypothesis that M-cells are basal or replacement cells provides an explanation for the
426 morphology and growth of the MGl in *M. brachydactyla*. In adults, several tubules of
427 variable length arise from a central tubule to create a ramified morphology. In late
428 megalopa and juveniles, the new tubules sprout from the lateral walls of existing tubules
429 (Fig. 3). In both cases, the emergence of new tubules can be explained if the MGl
430 contains basal cells; i.e., a cell type that remains dormant in the tubule walls, which

when stimulated by physiological processes differentiates into E-cells that will form a new tubule from the walls of an existing tubule. In addition, at the ultrastructural level, M-cells share numerous similarities with the basal cells of the midgut tract and midgut caeca of *M. brachydactyla* such as small size, rounded shape, and cytoplasm poor in organelles (Castejón et al., 2018), and with the basal cells of the midgut tract and midgut caeca of other decapods (Pugh, 1962; Komuro and Yamamoto, 1968).

In conclusion, the role of midgut gland of *M. brachydactyla* is similar throughout the entire lifespan of the spider crab because similar cell organization and morphology is observed in all stages. During development, the main change in the midgut gland is a significant increase in the size and number of tubules and a larger size of the epithelial cells, which increases the capacity of the midgut gland to process large volumes and diversity of food.

Acknowledgements

Financial support was provided by the Spanish Ministry of Economy and Competitiveness through the INIA project [grant number RTA2011-00004-00-00] to G.G and a predoctoral fellowship to D.C. [FPI-INIA]. The authors thank the technicians at IRTA in Sant Carles de la Ràpita (David Carmona, Glòria Macià, Magda Monllaó, Francesc X. Ingla and Olga Bellot) and at CCiTUB in Hospital Clinic, Barcelona (Adriana Martínez, Almudena García, José Manuel Rebled, Rosa Rivera) for their assistance. We thank the staff of Bruker SkyScan for their effectiveness and timely support, their continuous improvements to the software, and for implementing the new options that we had requested. In that respect, we are especially indebted to Alexander Sasov, Stephan Boons, Xuan Liu, Phil Salmon, and Vladimir Kharitonov.

Figure Legends.

Figure 1. *Maja brachydactyla*. Micro-CT volume rendering CTVox's reconstruction images. Megalopa. Entire specimen (A-B): dorsal view (A); lateral view (B). Midgut gland, close view (C-D): dorsal view (C); lateral view (D). Abbreviations: A ➤ P, anterior ➤ posterior; ANC, abdominal nerve cord; CS, cardiac stomach; H, heart; HT, hindgut tract; M, muscles; MT, midgut tract; PC, posterior caecum; MGl, midgut gland; PS, pyloric stomach; TG, thoracic ganglia.

Figure 2. *Maja brachydactyla*. Midgut gland. Gross morphology. Adult, dorsal view, digital camera (A). Zoea I, SEM: dorsal (B) and lateral view (C). Adult, blind-end tubules, SEM (D). Adult, muscle network, SEM (E). Abbreviations: AP, anterior projection; CM, circular muscles; CT, central tubule; DSL, dorsal sub-lobule; ET, external tubule; HT, hindgut tract; IT, internal tubule; LM, longitudinal muscles; LP, lateral projection; MGl, midgut gland; PP, posterior projection; Sto, stomach; VSL, ventral sub-lobule.

Figure 3. *Maja brachydactyla*. Diagrams showing different views (ventral, dorsal and lateral) of the larval midgut gland at the start of different stages (zoea I, zoea II, megalopa and first juvenile).

Figure 4. *Maja brachydactyla*. Midgut gland. Histology. Tubule, longitudinal section: adult stained with Hematoxylin-Eosin (A), and megalopa stained with Mallory's Trichrome (B). Tubule, transversal section, Hematoxylin-Eosin: adult (C), and zoea I (D). Adult, E-cells, Hematoxylin-Eosin (E). Adult, M-cells, Mallory's trichrome (F). Abbreviations: BC, B-cells; BM, basement membrane; CM, circular muscles; FC, F-cells; MC, M-cells; MV, microvilli; RC, R-cells.

Figure 5. *Maja brachydactyla*. Midgut gland. Histology. Epithelial cells. Larval and first juvenile stages, general diagram (A). Zoea I, Hematoxylin-Eosin (B). Megalopa, Mallory's trichrome (C). Megalopa, B-cell, Mallory's trichrome (D). Megalopa, E-cells, PAS contrasted with Methylene Blue (E). Adult, general diagram (F). Adult, epithelial cells: Hematoxylin-Eosin (G) and Mallory's trichrome (H). Abbreviations: BC, B-cells; BM, basement membrane; EC, E-cells; FC, F-cells; MC, M-cell; MF, muscle fibers; MV, microvilli; RC, R-cells.

Figure 6. *Maja brachydactyla*. Midgut gland. Ultrastructure of the R-cells. TEM. General diagram (A). Megalopa, general view (B). Cell apex: megalopa (C), and adult (D). Cell basis: megalopa (E), and adult (F). Golgi body, close view (G). Fusion of the SER with the basal membrane (arrows): megalopa (H), and adult (I). Abbreviations: BF, basal folds; BL, basal lamina; CJ, cell-to-cell junctions; FS, filamentous structures; LD, lipid droplets; M, mitochondria; MV, microvilli; N, nucleus; RER, rough endoplasmic reticulum; SER, smooth endoplasmic reticulum.

Figure 7. *Maja brachydactyla*. Midgut gland. Ultrastructure of the F-cells. TEM. General diagram (A). Megalopa, cell apex (B). Adult, supranuclear region (C). Adult, infranuclear region and cell basis (D). Abbreviations: BL, basal lamina; FS, filamentous structures; G, Golgi bodies; M, mitochondria; MV, microvilli; N, nucleus; RER, rough endoplasmic reticulum; SER, smooth endoplasmic reticulum.

Figure 8. *Maja brachydactyla*. Midgut gland. Ultrastructure of the B-cells. TEM. General diagram (A). Cell apex, supra-vacuolar region (B). Megalopa, general view (C). Micro-apocrine secretion (numbered) (D). Golgi body (E). Content of the central vacuole (F). Abbreviations: CJ, cell-to-cell junction; CV, central vacuole; G, Golgi

bodies, M: mitochondria; MV, microvilli; MVs, micro-vesicles; N, nucleus; RER, rough endoplasmic reticulum.

Figure 9. *Maja brachydactyla*. Midgut gland. Ultrastructure of the M-cells. TEM. General diagram (A). General view of the M-cells (B-C): adult (B) and megalopa (C). Golgi body (D). Annulated lamellae and pores (arrows) (E). Electron-dense vesicle (F). Abbreviations: BL, basal lamina; EV, electron-dense vesicles; G, Golgi bodies; M, mitochondria; N, nucleus.

Suppl. Fig. 1. *Maja brachydactyla*. Midgut gland. Larvae. Diagrams showing the measures taken for the morphometric study. Abbreviations: DSL, dorsal sub-lobule; DSh, dorsal sub-lobule height; DSl, dorsal sub-lobule length; DSw, dorsal sub-lobule width; ET, external tubule; ETl, external tubule length; ETw, external tubule width; IT, internal tubule; ITl, internal tubule length; ITw, internal tubule width; VSL, ventral sub-lobule; MW, maximum width; TL, total length.

Suppl. Fig. 2. *Maja brachydactyla*. Larvae. Location of the midgut gland. Dissecting microscope. Zoea I, lateral view (A). Zoea II, dorsal view (B). Zoea I, dissected midgut gland and adjacent organs (C). Megalopa, lateral view (D). Megalopa, dorsal view (E). Megalopa, dissected midgut gland and adjacent organs (F). Abbreviations: HT, hindgut tract; MT, midgut tract; MGl, midgut gland; Sto, stomach.

Suppl. Fig. 3. *Maja brachydactyla*. Midgut gland. Tomographic and microtomographic cross section images. Adult tomography, female. The midgut gland is marked by the dotted line (A-B): anatomical area of the stomach (A) and anatomical area of the heart (B). Larvae, Micro-CT Data Viewer's cross section images, the midgut gland is marked by the dotted line (C-D): zoea I, anatomical area of the pyloric stomach

(C) and megalopa, anatomical area of the pyloric stomach (D). Abbreviations: BC, branchial chamber; MT, midgut tract; MGl, midgut gland; Sto, stomach.

Suppl. Fig. 4. *Maja brachydactyla*. Midgut gland. Larvae. Close view of the musculature. Abbreviations: CL, circular musculature; LM, longitudinal musculature.

Suppl. Fig. 5. *Maja brachydactyla*. Midgut gland. Transitional cell: F-cell with features of B-cell (A-C). General view (A). Rough endoplasmic reticulum (B). Vacuole content, partially digested mitochondria (C).

References

Abrunhosa, F.A., Kittaka, J., 1997. Morphological changes in the midgut, midgut gland and hindgut during the larval and postlarval development of the red king crab *Paralithodes camtschaticus*. Fisheries Science 63, 746-754.

Al-Mohanna, S.Y., Nott, J.A., 1986. B-cells and digestion in the hepatopancreas of *Penaeus semisulcatus* (Crustacea: Decapoda). Journal of the Marine Biological Association of the United Kingdom 66, 403-414.

Al-Mohanna, S.Y., Nott, J.A., 1987. R-cells and the digestive cycle in *Penaeus semisulcatus* (Crustacea: Decapoda). Marine Biology 95, 129-137.

Al-Mohanna, S.Y., Nott, J.A., 1989. Functional cytology of the hepatopancreas of *Penaeus semisulcatus* (Crustacea: Decapoda) during the moult cycle. Marine Biology 101, 535-544.

Al-Mohanna, S.Y., Nott, J.A., Lane, D.J.W., 1985a. M-'Midget' cells in the hepatopancreas of the shrimp, *Penaeus semisulcatus* De Hann, 1844 (Decapoda, Natantia). Crustaceana 48, 260-268.

Al-Mohanna, S.Y., Nott, J.A., Lane, D.J.W., 1985b. Mitotic E- and secretory F-cells in the hepatopancreas of the shrimp *Penaeus semisulcatus* (Crustacea: Decapoda). Journal of the Marine Biological Association of the United Kingdom 65, 901-910.

Alba-Tercedor, J., 2014. From the sample preparation to the volume rendering images of small animals: A step by step example of a procedure to carry out the micro-CT study of the leafhopper insect *Homalodisca vitripennis* (Hemiptera: Cicadellidae), in: Skyscan (Ed.), Bruker microCT Users Meeting 2014, Kontich, Belgium, pp. 260-288.

Alba-Tercedor, J., Alba-Alejandre, I., 2017. Comparing micro-CT results of insects with classical anatomical studies: The European honey bee (*Apis mellifera* Linnaeus, 1758) as a benchmark

(Insecta: Hymenoptera, Apidae), in: Skyscan (Ed.), Micro-CT User Meeting 2017, Kontich, Belgium, pp. 147-167.

Alba-Tercedor, J., Sáinz-Cantero, C.E., 2012. Volume rendering reconstructions of the anatomy of small aquatic beetles (Insecta : Coleoptera) scanned with the Skyscan 1172 high resolution micro-CT, in: Skyscan (Ed.), Micro-CT Users Meeting 2012, Kontich, Belgium, pp. 75-84.

Andrés, M., Gisbert, E., Díaz, M., Moyano, F.J., Estévez, A., Rotllant, G., 2010. Ontogenetic changes in digestive enzymatic capacities of the spider crab, *Maja brachydactyla* (Decapoda: Majidae). Journal of Experimental Marine Biology and Ecology 389, 75-84.

Anger, K., Storch, V., Anger, V., Capuzzo, J.M., 1985. Effects of starvation on moult cycle and hepatopancreas of stage I lobster (*Homarus americanus*) larvae. Helgoländer Meeresuntersuchungen 39, 107-116.

Barker, P.L., Gibson, R., 1977. Observations on the feeding mechanism, structure of the gut, and digestive physiology of the european lobster *Homarus gammarus* (L.) (Decapoda: Nephropidae). Journal of Experimental Marine Biology and Ecology 26, 297-324.

Barker, P.L., Gibson, R., 1978. Observations on the structure of the mouthparts, histology of the alimentary tract, and digestive physiology of the mud crab *Scylla serrata* (Forskål) (Decapoda: Portunidae). Journal of Experimental Marine Biology and Ecology 32, 177-196.

Biesiot, P.M., McDowell, J.E., 1995. Midgut-gland development during early life-history of the American Lobster *Homarus americanus*. Journal of Crustacean Biology 15, 679-685.

Bolognesi, R., Ribeiro, A.F., Terra, W.R., Ferreira, C., 2001. The peritrophic membrane of *Spodoptera frugiperda*: Secretion of peritrophins and role in immobilization and recycling digestive enzymes. Archives of Insect Biochemistry and Physiology 47, 62-75.

Bunt, A.H., 1968. An ultrastructural study of the hepatopancreas of *Procambarus clarkii* (Girard) (Decapoda, Astacidea). Crustaceana 15, 282-288.

Castejón, D., Alba-Tercedor, J., Rotllant, G., Ribes, E., Durfort, M., Guerao, G., 2018. Micro-computed tomography and histology to explore internal morphology in decapod larvae. Scientific Reports 8, 14399.

Cervellione, F., McGurk, C., Silva, P., Owen, M.A.G., Van den Broeck, W., 2017a. Optimization of fixation methods for image analysis of the hepatopancreas in whiteleg shrimp, *Penaeus vannamei* (Boone). Journal of Fish Diseases 40, 517-527.

Cervellione, F., McGurk, C., Van den Broeck, W., 2017b. “Perigastric organ”: a replacement name for the “hepatopancreas” of Decapoda. Journal of Crustacean Biology 37, 353-355.

586 Cristofoletti, P.T., Ribeiro, A.F., Terra, W.R., 2001. Apocrine secretion of amylase and exocytosis of
587 trypsin along the midgut of *Tenebrio molitor* larvae. Journal of Insect Physiology 47, 143-155.

588 Cuartas, E., Petriella, A.M., 2002. Cytoarchitecture of the hepatopancreas of three species of crabs from
589 Mar Chiquita Lagoon, Argentina, In: Escobar-Briones, E., Alvarez, F. (Eds.), Modern
590 Approaches to the Study of Crustacea. Springer US, Boston, MA, pp. 39-44.

591 Davie, P.J.F., Guinot, D., Ng, P.K.L., 2015. Anatomy and functional morphology of Brachyura, in:
592 Castro, P., Davie, P.J.F., Guinot, D., Schram, F., Von Vaupel Klein, C. (Eds.), Treatise on
593 Zoology - Anatomy Taxonomy Biology. The Crustacea Volume 9 Part C. Brill, pp. 11-163.

594 Erri Babu, D., Shyamasundari, K., Rao, K.H., 1982. Studies on the digestive system of the crab *Menippe*
595 *rumphii* (Fabricius) (Crustacea:Brachyura). Journal of Experimental Marine Biology and
596 Ecology 58, 175-191.

597 Felgenhauer, B.E., 1992. Chapter 3. Internal Anatomy of the Decapoda: An Overview, In: Harrison,
598 F.W., Humes, A.G. (Eds.), Microscopic Anatomy of Invertebrates. Volume 10: Decapod
599 Crustacea. Wiley-Liss, Inc., pp. 45-75.

600 Ferreira, C., Bellinello, G.L., Ribeiro, A.F., Terra, W.R., 1990. Digestive enzymes associated with the
601 glycocalyx, microvillar membranes and secretory vesicles from midgut cells of *Tenebrio molitor*
602 larvae. Insect Biochemistry 20, 839-847.

603 Franceschini-Vicentini, I.B., Ribeiro, K., Papa, L.P., Marques Junior, J., Vicentini, C.A., Valenti,
604 P.M.C.M., 2009. Histoarchitectural features of the hepatopancreas of the Amazon River Prawn
605 *Macrobrachium amazonicum*. International Journal of Morphology 27, 121-128.

606 Gibson, R., Barker, P.L., 1979. The Decapod Hepatopancreas. Oceanography and Marine Biology - An
607 Annual Review 17, 285-346.

608 Guerao, G., Simeó, C.G., Anger, K., Urzúa, Á., Rotllant, G., 2012. Nutritional vulnerability of early zoea
609 larvae of the crab *Maja brachydactyla* (Brachyura, Majidae). Aquatic Biology 16, 253-264.

610 Hopkin, S.P., Nott, J.A., 1979. Some observations on concentrically structured, intracellular granules in
611 the hepatopancreas of the shore crab *Carcinus maenas* (L.). Journal of the Marine Biological
612 Association of the United Kingdom 59, 867-877.

613 Hopkin, S.P., Nott, J.A., 1980. Studies on the digestive cycle of the shore crab *Carcinus maenas* (L.) with
614 special reference to the b cells in the hepatopancreas. Journal of the Marine Biological
615 Association of the United Kingdom 60, 891-907.

616 Hu, K.-J., Leung, P.-C., 2007. Food digestion by cathepsin L and digestion-related rapid cell
617 differentiation in shrimp hepatopancreas. Comparative Biochemistry and Physiology Part B:
618 Biochemistry and Molecular Biology 146, 69-80.

619 Icely, J.D., Nott, J.A., 1992. Digestion and absorption: digestive system and associated organs, In:
620 Harrison, F.W., Humes, A.G. (Eds.), Microscopic anatomy of invertebrates: decapod Crustacea.
621 Wiley-Liss, New York, pp. 147-201.

622 Jantrarotai, P.N., Sawanyatiputi, S.A., 2005. Histological study on the development of digestive system in
623 zoeal stages of mud crab (*Scylla olivacea*). Kasetsart Journal 39, 666-671.

624 Johnston, M.D., 2006. Feeding and digestion in the phyllosoma larvae of Ornate Spiny Lobster,
625 *Panulirus ornatus* (Fabricius) and the implications for their culture, Zoology. The University of
626 Western Australia, p. 146.

627 Komuro, T., Yamamoto, T., 1968. Fine structure of the epithelium of the gut in the crayfish
628 (*Procambarus clarkii*) with special reference to the cytoplasmic microtutubles. Archivum
629 histologicum japonicum 30, 17-32.

630 Li, F., Li, S., 1998. Studies on the hepatopancreas of larval *Scylla serrata*. Oceanologia Et Limnologia
631 Sinica 29, 29-34.

632 Loizzi, R.F., 1971. Interpretation of crayfish hepatopancreatic function based on fine structural analysis
633 of epithelial cell lines and muscle network. Zeitschrift für Zellforschung und Mikroskopische
634 Anatomie 113, 420-440.

635 Mikami, S., Greenwood, J.G., Takashima, F., 1994. Functional morphology and cytology of the
636 phyllosomal digestive system of *Ibacus ciliatus* and *Panulirus japonicus* (Decapoda, Scyllaridae
637 and Palinuridae). Crustaceana 67, 212-225.

638 Milne-Edwards, H., 1834a. Histoire naturelle des crustacés, comprenant l'anatomie, la physiologie et la
639 classification de ces animaux. Libraire Encyclopédique de Roret.

640 Milne-Edwards, H., 1834b. Histoire naturelle des crustacés: atlas. Libraire Encyclopédique de Roret.

641 Monteiro, E.C., Tamaki, F.K., Terra, W.R., Ribeiro, A.F., 2014. The digestive system of the “stick bug”
642 *Cladomorphus phyllinus* (Phasmida, Phasmatidae): A morphological, physiological and
643 biochemical analysis. Arthropod Structure & Development 43, 123-134.

644 Nakamura, K., 1990. Organogenesis during metamorphosis in the swimming crab *Portunus*
645 *trituberculatus*. Nippon Suisan Gakkaishi 56, 1561-1564.

646 Nishida, S., Takahashi, Y., Kittaka, J., 1995. Structural changes in the hepatopancreas of the rock lobster,
647 *Jasus edwardsii* (Crustacea: Palinuridae) during development from the puerulus to post-
648 puerulus. Marine Biology 123, 837-844.

649 Nunes, E.T., Braga, A.A., Camargo-Mathias, M.I., 2014. Histochemical study of the hepatopancreas in
650 adult females of the pink-shrimp *Farfantepenaeus brasiliensis* Latreille, 1817. Acta
651 Histochemica 116, 243-251.

652 Paquet, F., Germain, P., Fritsch, P., 1993. Étude ultra-structurale de la glande digestive du homard
653 *Homarus gammarus*. Rôle des divers types cellulaires dans les processus digestifs. Cahiers de
654 Biologie Marine 35, 15-37.

655 Pillai, R.S., 1960. Studies on the shrimp *Caridina laevis* (Heller) 1. The Digestive System. Journal of the
656 Marine Biological Association of India 2, 57-74.

657 Pugh, J.E., 1962. A contribution toward a knowledge of the hind-gut of fiddler crabs (Decapoda,
658 Grapsidae). Transactions of the American Microscopical Society 81, 309-320.

659 R Development Core Team, 2015. R: A language and environment for statistical computing. R
660 Foundation for Statistical Computing, Vienna, Austria.

661 Ramadevi, K.R.L.S., Shyamasundari, K., Hanumantha Rao, K., 1990. Observation of the hepatopancreas
662 of *Ocypoda platytarsis* (Milne-Edwards) (Crustacea, Brachyura). Bolletino di zoologia 57, 261-
663 265.

664 Reddy, A.R., 1937. The physiology of digestion and absorption in the crab *Paratelphusa* (*Oziotelphusa*)
665 *hydrodromus* (Herbst). Proceedings of the Indian Academy of Sciences - Section B 6, 170-193.

666 Reddy, A.R., 1938. The cytology of digestion and absorption in the crab *Paratelphusa* (*Oziotelphusa*)
667 *hydrodromus* (Herbst). Proceedings of the Indian Academy of Sciences - Section B 8, 171-181.

668 Rotllant, G., Moyano, F.J., Andrés, M., Díaz, M., Estévez, A., Gisbert, E., 2008. Evaluation of
669 fluorogenic substrates in the assessment of digestive enzymes in a decapod crustacean *Maja*
670 *brachydactyla* larvae. Aquaculture 282, 90-96.

671 Rotllant, G., Moyano, F.J., Andrés, M., Estévez, A., Díaz, M., Gisbert, E., 2010. Effect of delayed first
672 feeding on larval performance of the spider crab *Maja brachydactyla* assessed by digestive
673 enzyme activities and biometric parameters. Marine Biology 157, 2215-2227.

674 Sánchez-Paz, A., García-Carreño, F., Hernández-López, J., Muhlia-Almazán, A., Yepiz-Plascencia, G.,
675 2007. Effect of short-term starvation on hepatopancreas and plasma energy reserves of the
676 Pacific white shrimp (*Litopenaeus vannamei*). Journal of Experimental Marine Biology and
677 Ecology 340, 184-193.

678 Schlegel, C., 1911. Anatomie sommaire de la première zoé de *Maja squinado* Latr. (Note préliminaire à
679 des recherches sur l'Organogénese des Décapodes brachyoures). Archives de Zoologie
680 Experimentale et Générale 5º Série T. VIII., 29-40.

Scholtz, G., Richter, S., 1995. Phylogenetic systematics of the reptantian Decapoda (Crustacea, Malacostraca). Zoological Journal of the Linnean Society 113, 289-328.

Silva, W., Cardoso, C., Ribeiro, A.F., Terra, W.R., Ferreira, C., 2013. Midgut proteins released by microapocrine secretion in *Spodoptera frugiperda*. Journal of Insect Physiology 59, 70-80.

Sonakowska, L., Włodarczyk, A., Poprawa, I., Binkowski, M., Śróbka, J., Kamińska, K., Kszuk-Jendrysik, M., Chajec, Ł., Zajusz, B., Rost-Roszkowska, M.M., 2015. Structure and Ultrastructure of the endodermal region of the alimentary tract in the freshwater shrimp *Neocaridina heteropoda* (Crustacea, Malacostraca). PLoS ONE 10, e0126900.

Spitzner, F., Meth, R., Krüger, C., Nischik, E., Eiler, S., Sombke, A., Torres, G., Harzsch, S., 2018. An atlas of larval organogenesis in the European shore crab *Carcinus maenas* L. (Decapoda, Brachyura, Portunidae). Frontiers in Zoology 15, 27.

Stanier, J.E., Woodhouse, M.A., Griffin, R.L., 1968. The Fine Structure of the Hepatopancreas of *Carcinus maenas* (L.) (Decapoda Brachyura). Crustaceana 14, 56-66.

Storch, V., Anger, K., 1983. Influence of starvation and feeding on the hepatopancreas of larval *Hyas araneus* (Decapoda, Majidae). Helgoländer Meeresuntersuchungen 36, 67-75.

Trask, T., 1974. Laboratory-reared larvae of *Cancer anthonyi* (Decapoda: Brachyura) with a brief description of the internal anatomy of the megalopa. Marine Biology 27, 63-74.

Travis, O.F., 1955. The molting cycle of the spiny lobster, *Panulirus argus* Latreille. II. Pre-ecdysial histological and histochemical changes in the hepatopancreas and integumental tissues. The Biological Bulletin 108, 88-112.

Van Weel, P.B., 1974. Hepatopancreas? Comparative Biochemistry and Physiology Part A: Physiology 47, 1-9.

Vogt, G., 1994. Life-cycle and functional cytology of the hepatopancreatic cells of *Astacus astacus* (Crustacea, Decapoda). Zoomorphology 114, 83-101.

Vogt, G., 1996. Morphology and physiology of digestive epithelia in Decapod crustaceans. Pflügers Archiv 431, R239-R240.

Williams, R.L., 1944. The pre-zoea stage of *Porcellana platycheles* (Pennant). Preliminary anatomical and histological notes. Journal of the Royal Microscopical Society 64, 1-15.

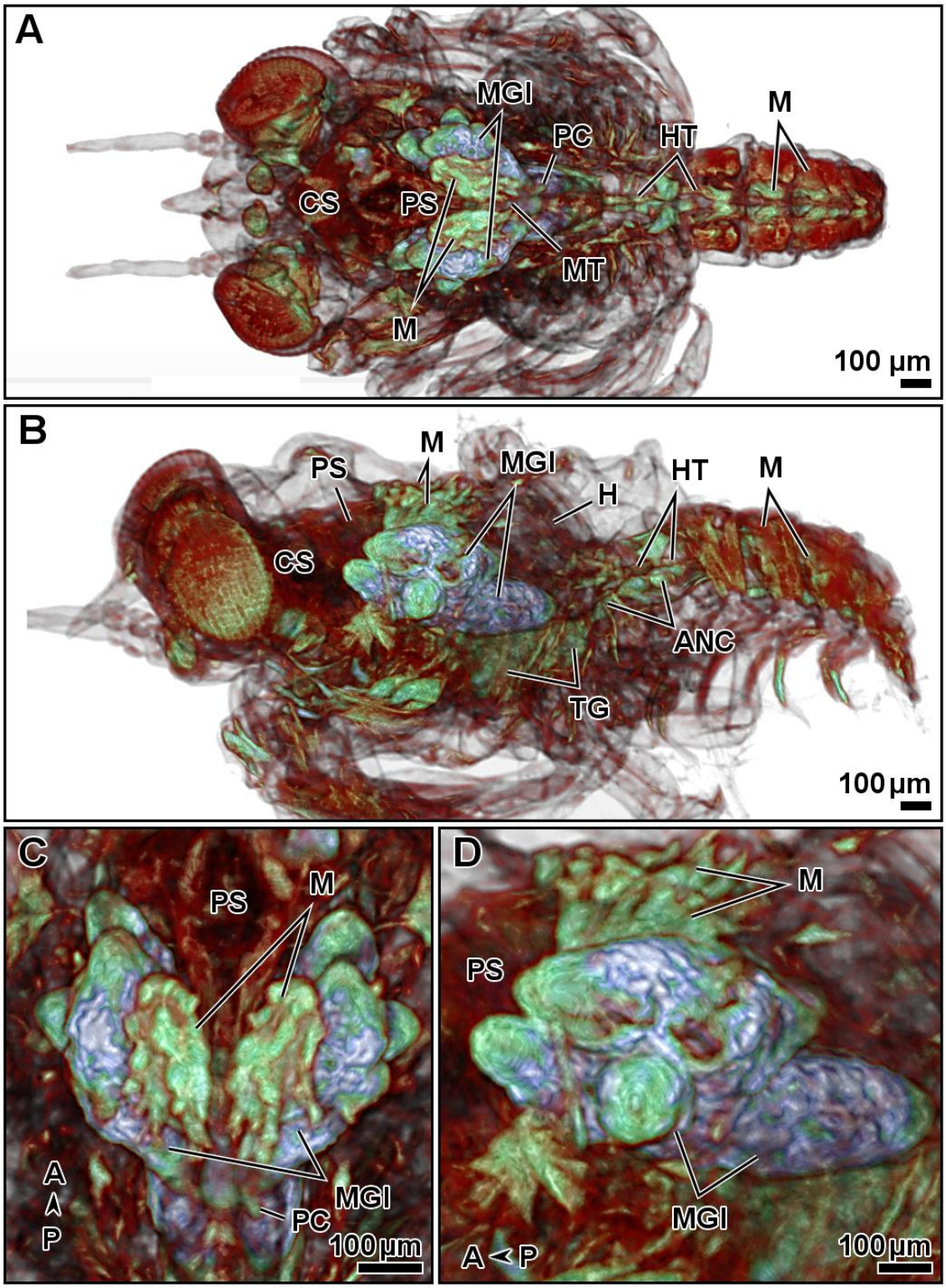
A
MGI
M
PC
HT
CS
PS
MT
M
100 µm
B
M
PS
MGI
HT
M
H
CS
ANC
TG
100 µm
C
PS
M
A
P
MGI
PC
100 µm
D
M
PS
MGI
A
P
100 µm

Figure 1

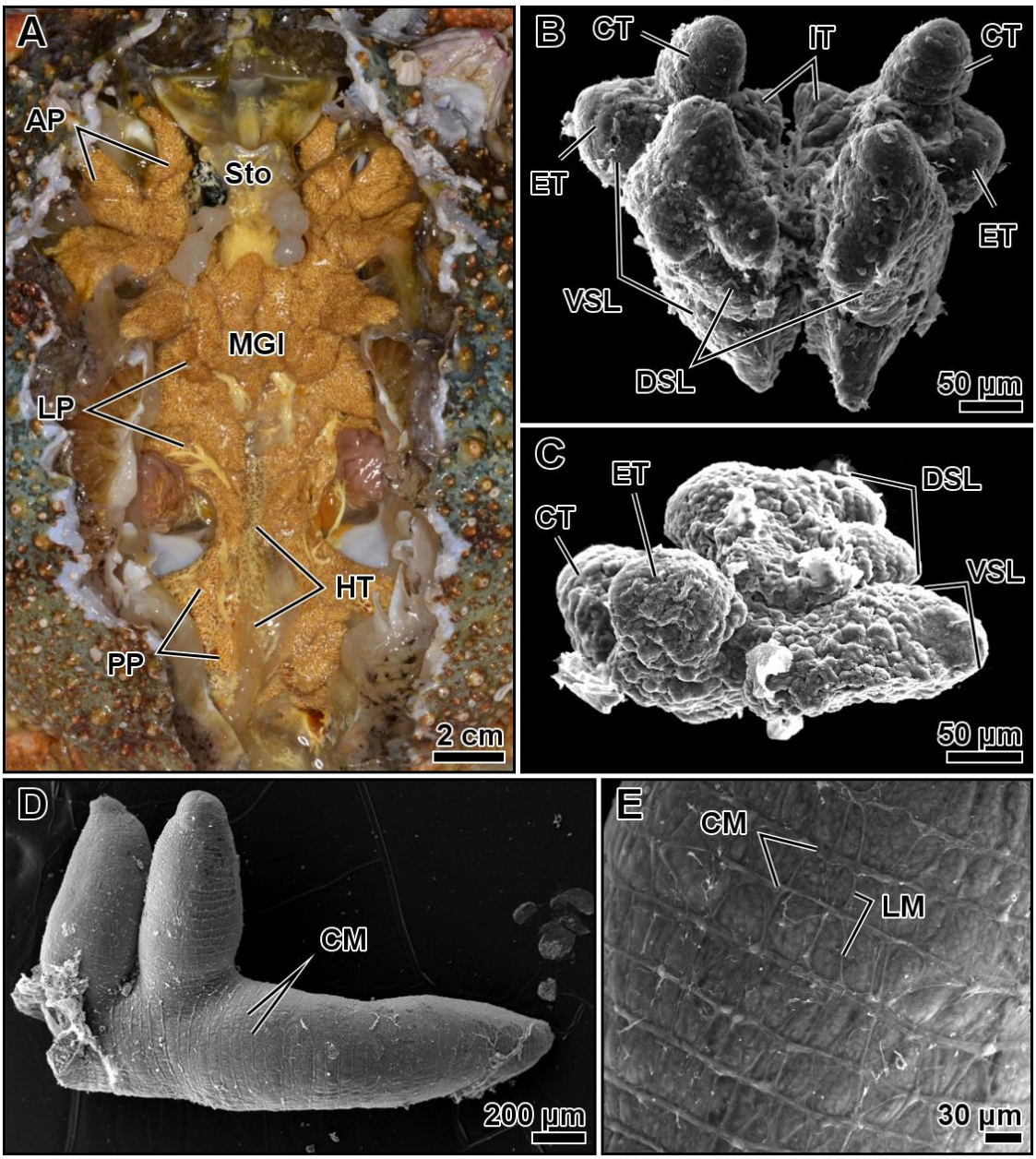
A
AP
Sto
MGI
LP
HT
PP
2 cm
B
CT
IT
CT
ET
ET
VSL
DSL
50 µm
C
ET
DSL
CT
VSL
50 µm
D
CM
200 µm
E
CM
LM
30 µm

Figure 2

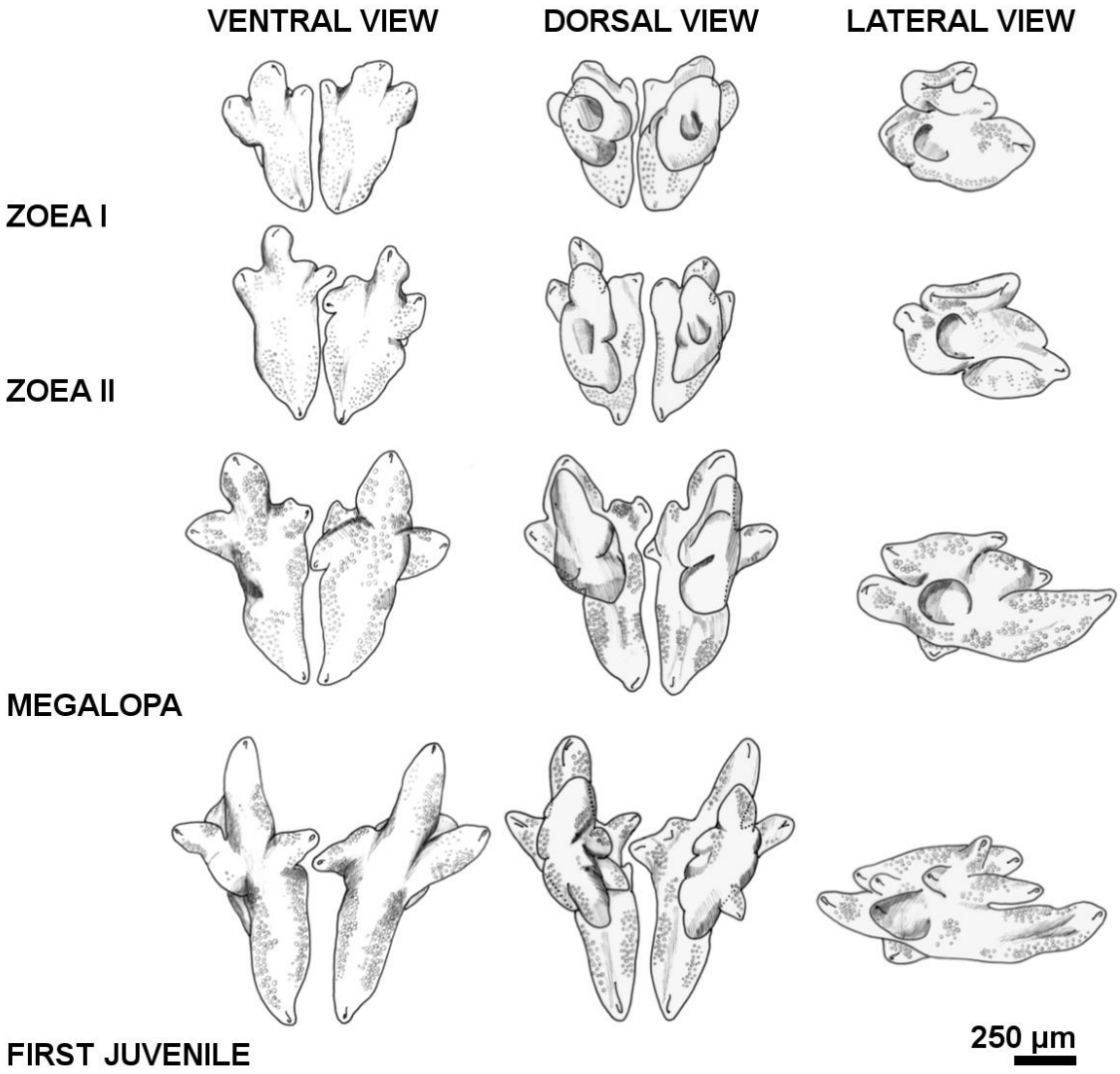

716
717 Figure 3
718

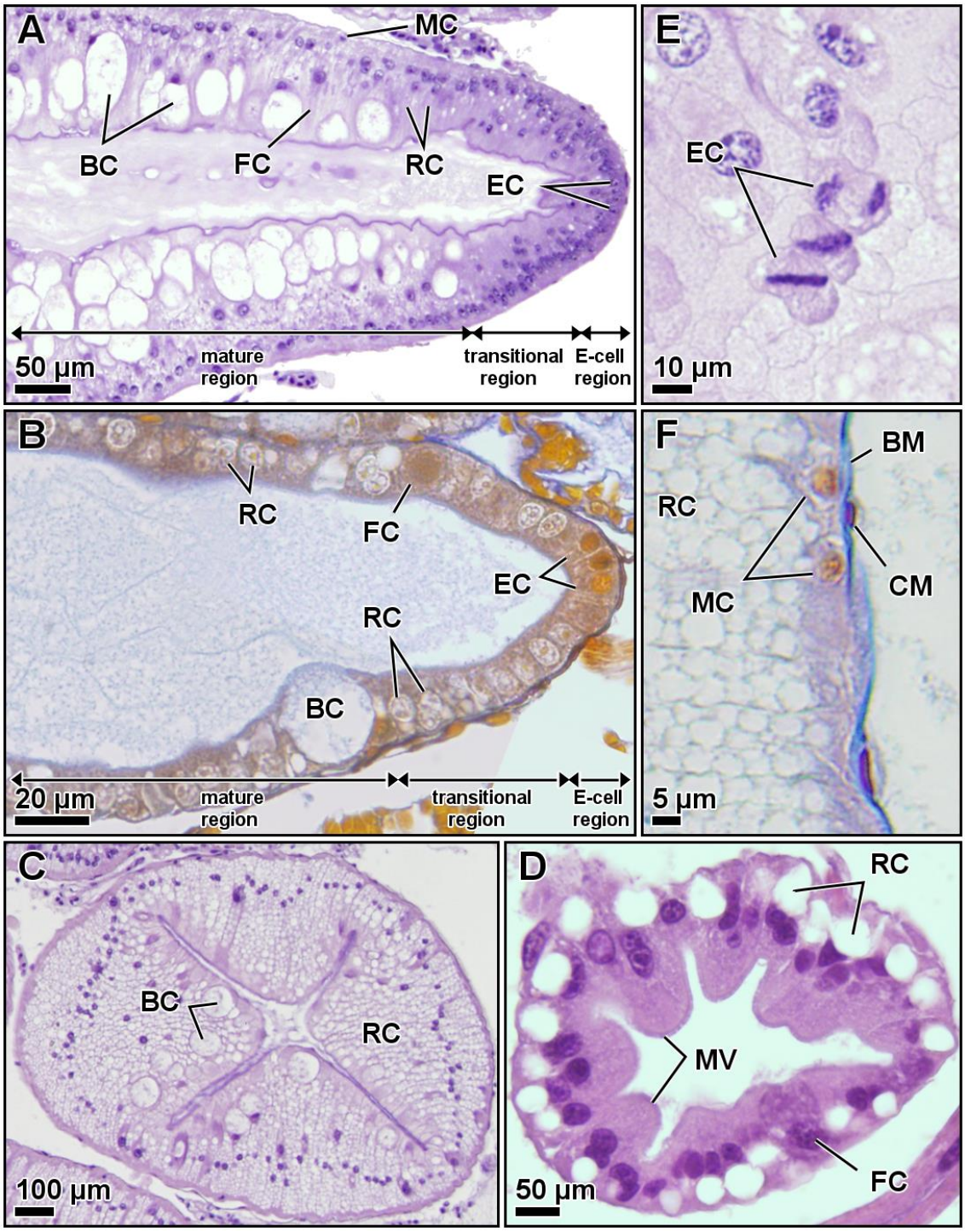
A
MC
BC
FC
RC
EC
50 µm
mature region
transitional region
E-cell region
E
EC
10 µm
B
RC
FC
EC
RC
BC
20 µm
mature region
transitional region
E-cell region
F
BM
RC
MC
CM
5 µm
C
BC
RC
100 µm
D
RC
MV
FC
50 µm

Figure 4

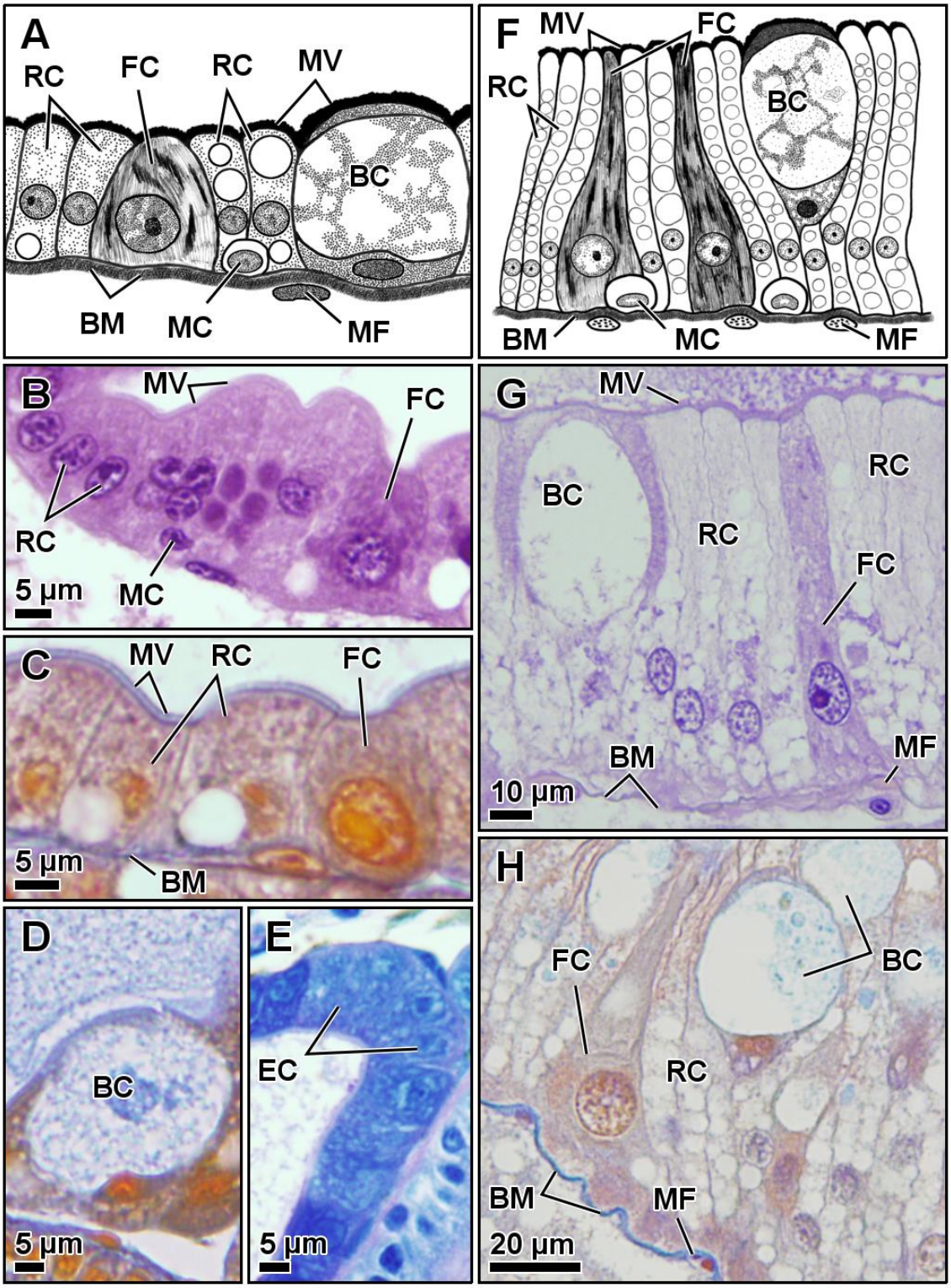
A
RC
FC
RC
MV
BC
BM
MC
MF
F
MV
FC
RC
BC
BM
MC
MF
B
MV
FC
RC
5 µm
MC
G
MV
BC
RC
RC
FC
BM
MF
10 µm
C
MV
RC
FC
5 µm
BM
H
FC
BC
RC
BM
MF
20 µm
D
BC
5 µm
E
EC
5 µm

Figure 5

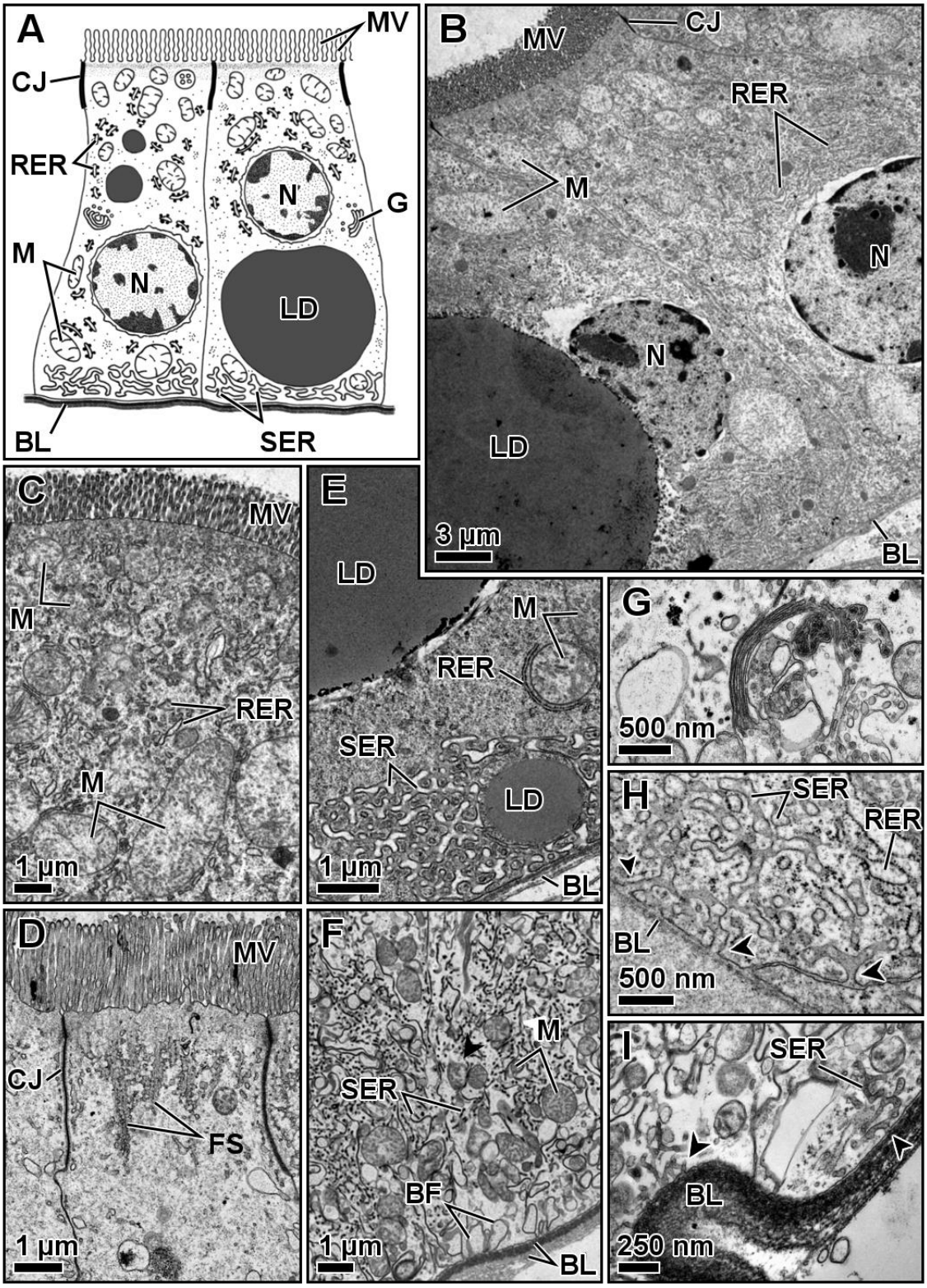
A
MV
CJ
RER
N
G
M
N
LD
BL
SER
B
MV
CJ
RER
M
N
N
LD
3 µm
BL
C
MV
M
RER
M
1 µm
E
LD
M
RER
SER
LD
1 µm
BL
G
500 nm
H
SER
RER
BL
500 nm
D
MV
CJ
FS
1 µm
F
M
SER
BF
1 µm
BL
I
SER
BL
250 nm

Figure 6

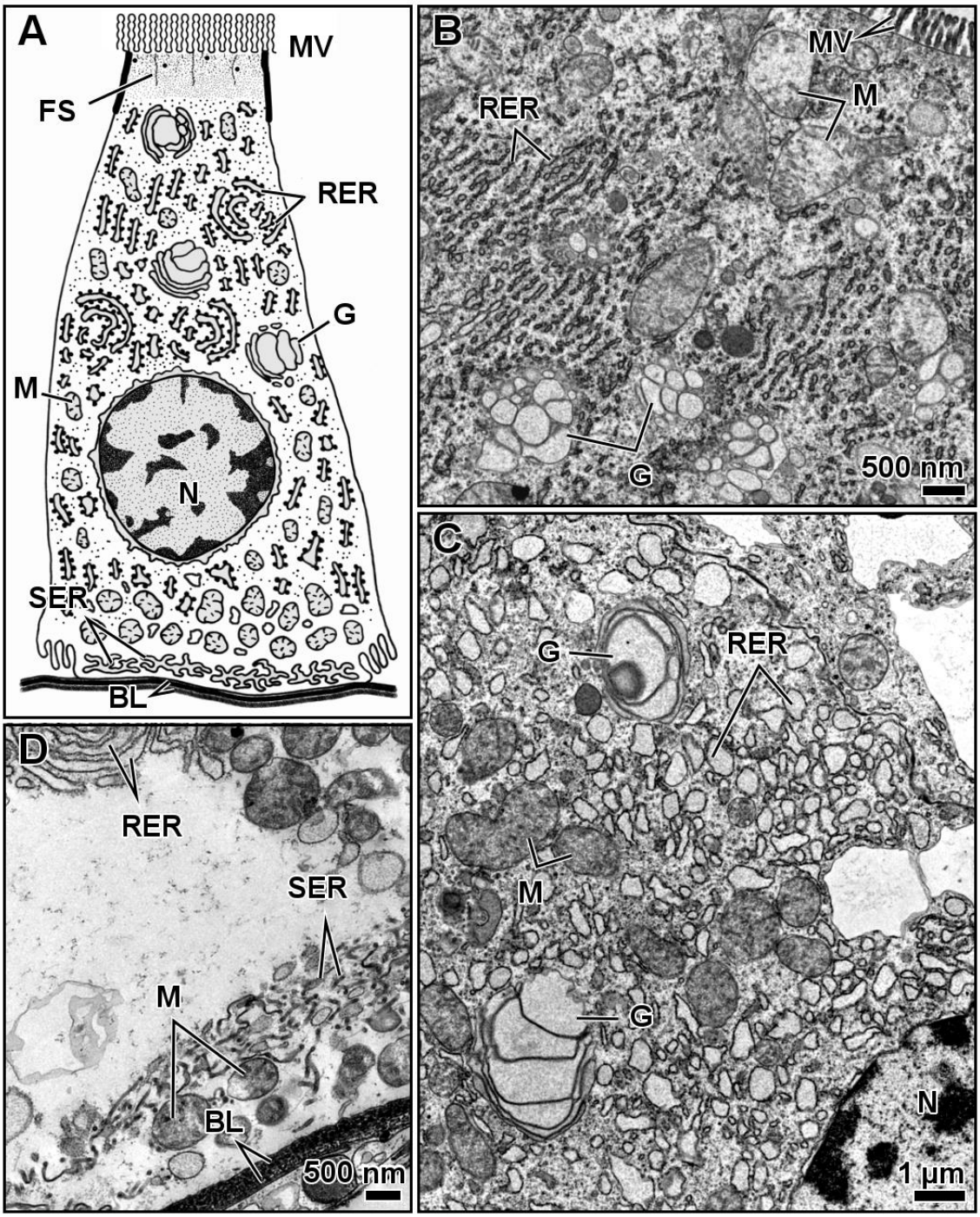
A
MV
FS
RER
G
M
N
SER
BL
B
MV
RER
M
G
500 nm
C
G
RER
M
G
N
1 µm
D
RER
SER
M
BL
500 nm

Figure 7

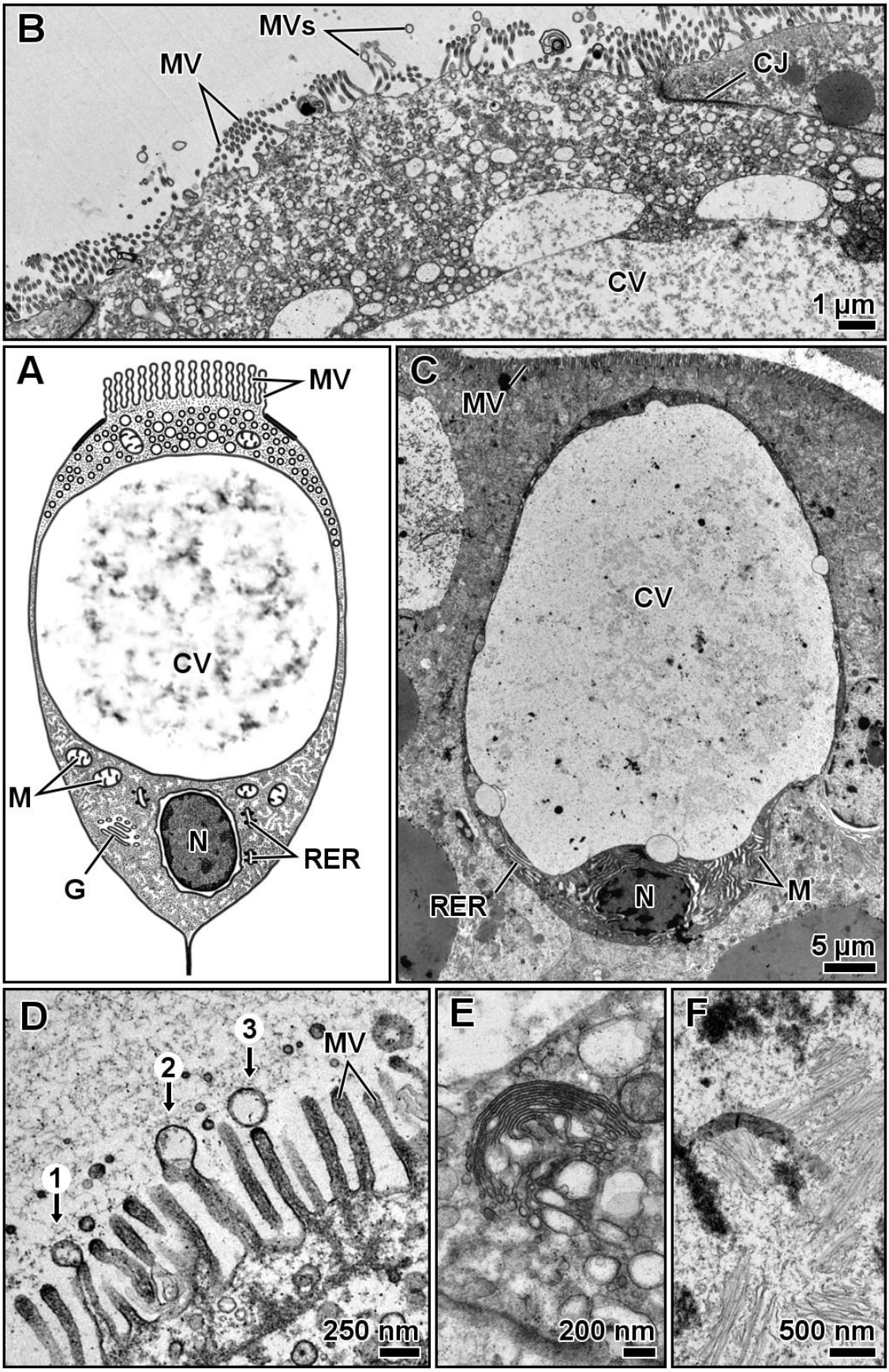
B
MVs
MV
CJ
CV
1 µm
A
MV
CV
M
N
RER
G
C
MV
CV
RER
N
M
5 µm
D
3
2
1
MV
250 nm
E
200 nm
F
500 nm

Figure 8

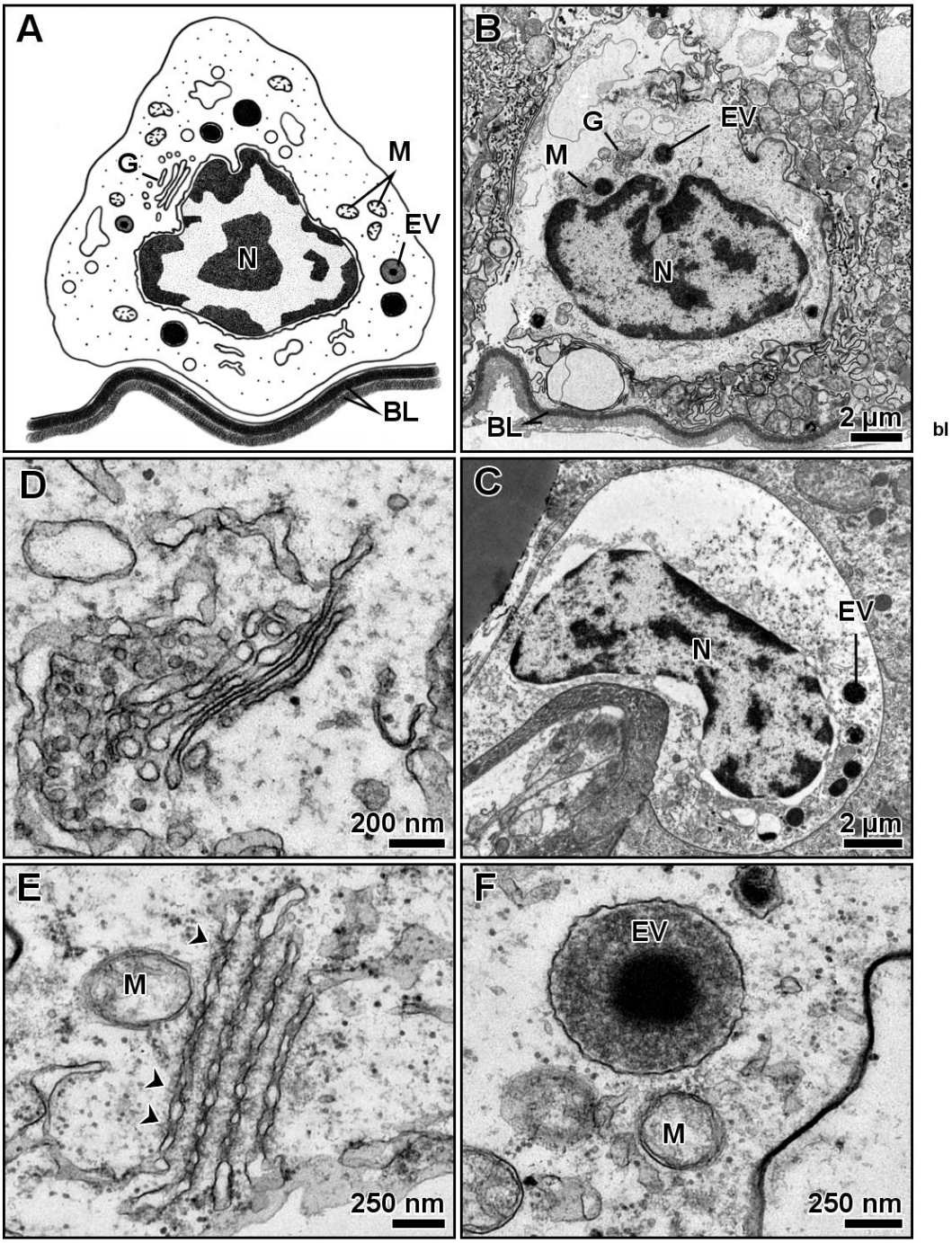
A
G
M
EV
N
BL
B
G
EV
M
N
BL
2 µm
bl
D
200 nm
C
EV
N
2 µm
E
M
250 nm
F
EV
M
250 nm

Figure 9

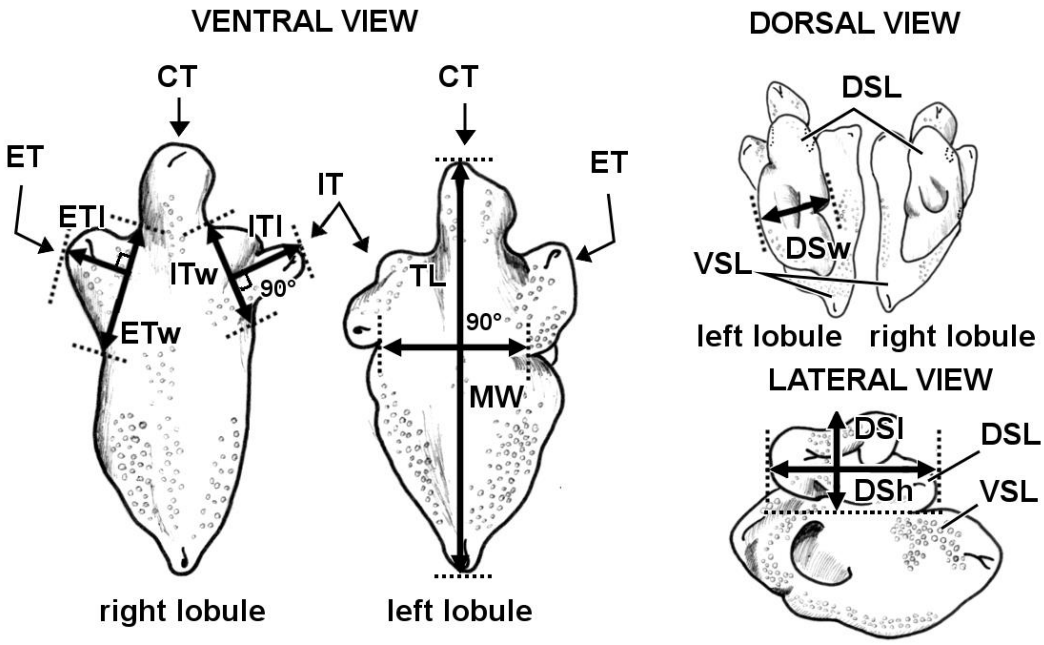

739

740 Supl. Figure 1

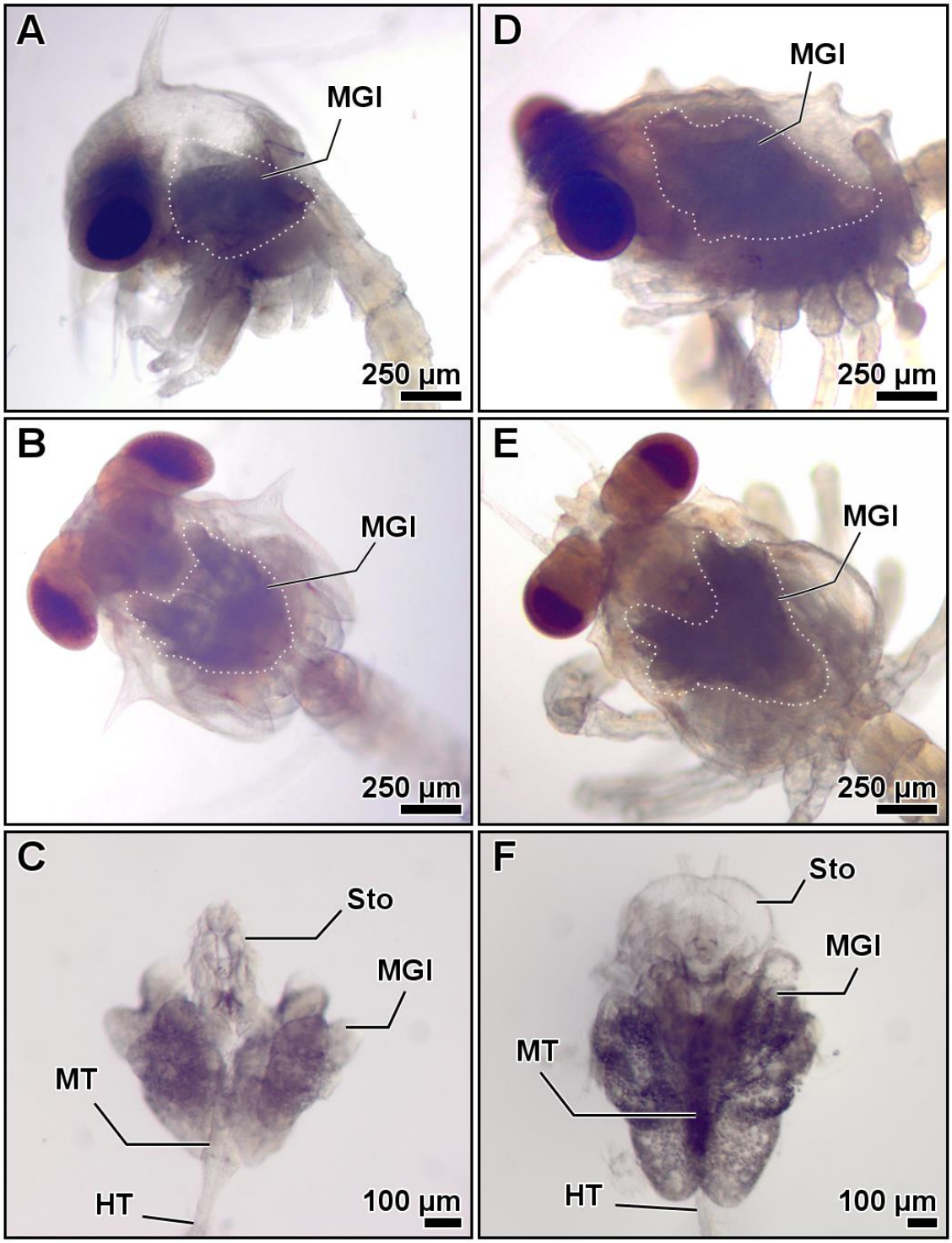

Supl. Figure 2

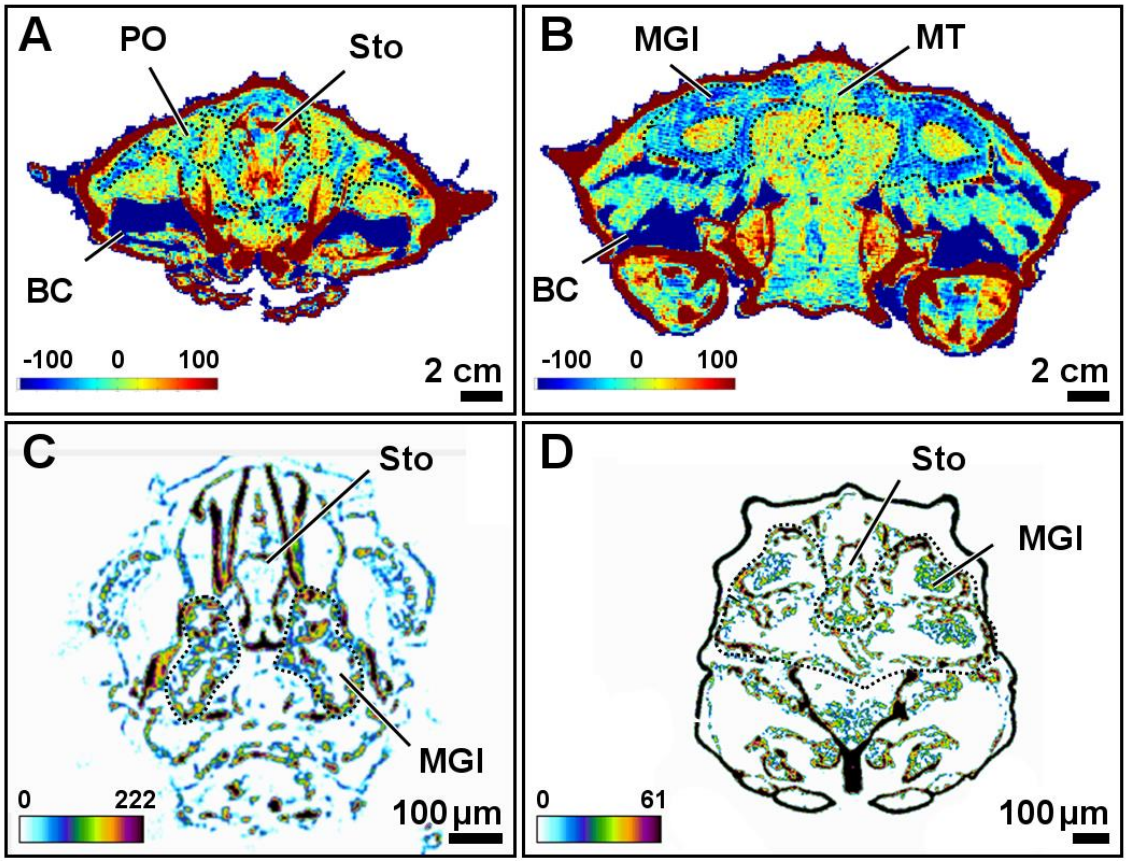

Supl. Figure 3

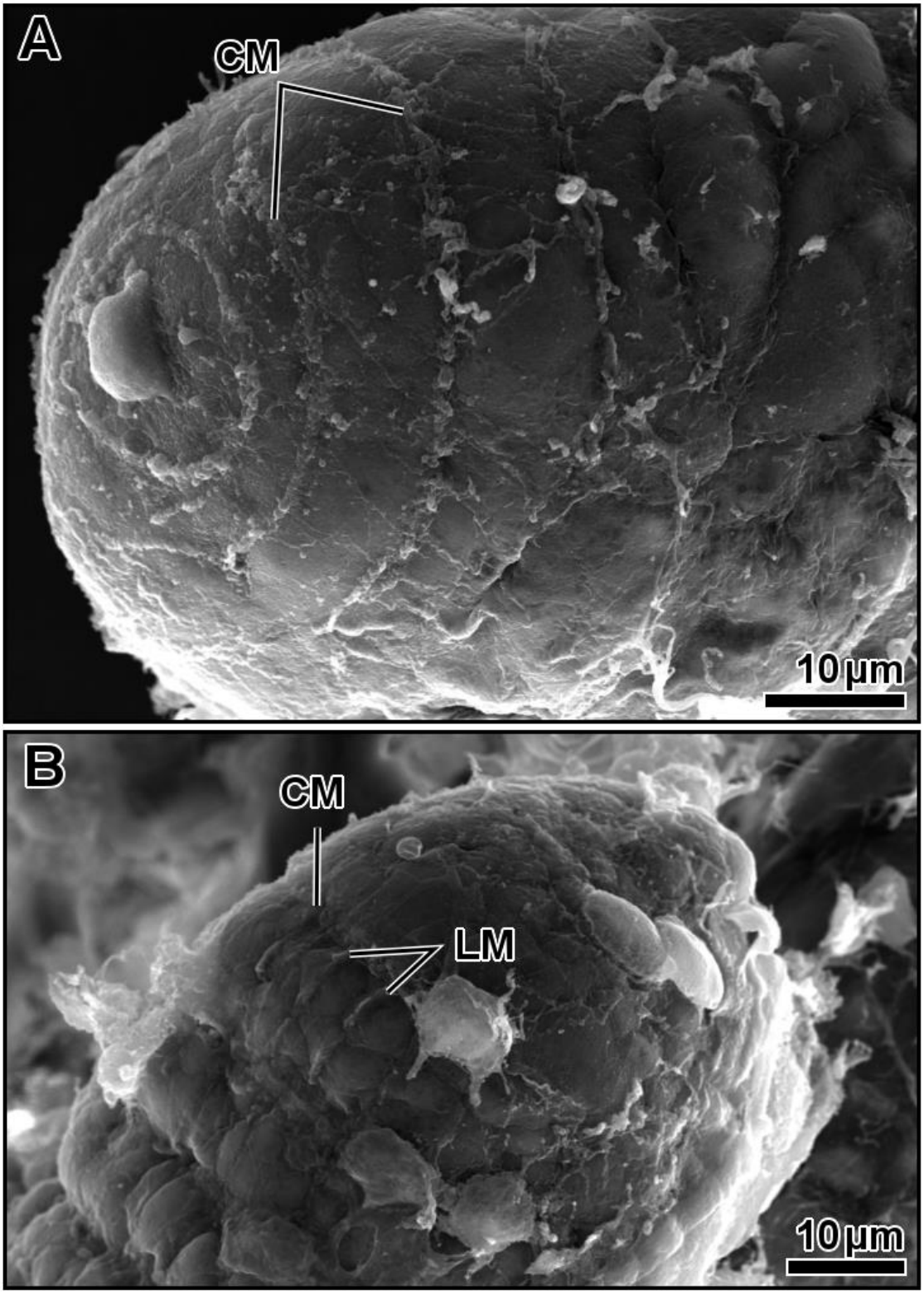

Supl. Figure 4

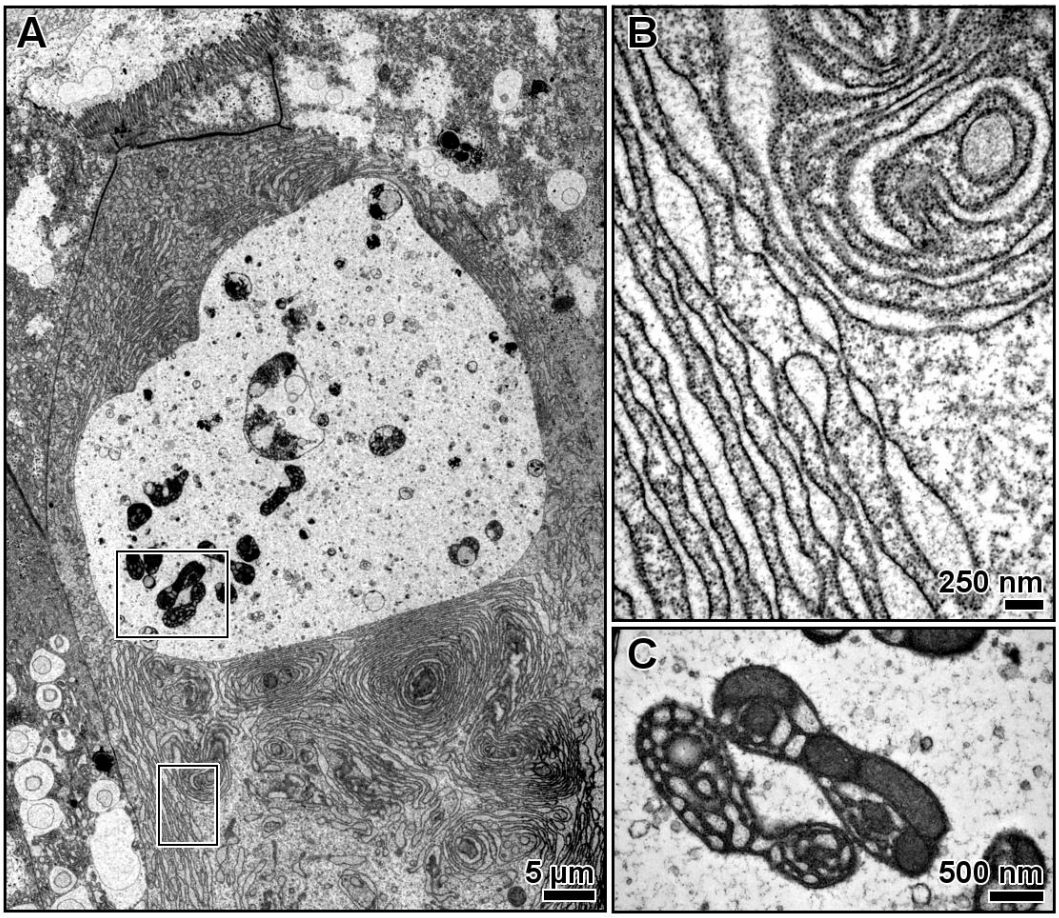

Supl. Figure 5